Transportation Research Part C 160 (2024) 104529

Contents lists available at ScienceDirect

Transportation Research Part C

journal homepage: www.elsevier.com/locate/trc

# Adaptive robust electric vehicle routing under energy consumption uncertainty

Jaehee Jeong [a,b], Bissan Ghaddar [b,c,*], Nicolas Zufferey [d], Jatin Nathwani [a]

[a] Department of Management Sciences, University of Waterloo, Waterloo, Ontario, Canada
[b] Ivey Business School of London, Canada
[c] Department of Technology, Management and Economics, Technical University of Denmark, Denmark
[d] Geneva School of Economics and Management, University of Geneva, Geneva, Switzerland

ARTICLE INFO

*Keywords:*
Adaptive robust optimization
Electric vehicle routing
Uncertainty
Decomposition
Mixed integer linear programming

ABSTRACT

Electric vehicles (EVs) have been highly favoured as a mode of transportation in recent years. EVs offer numerous benefits over traditional fuel-based vehicles, particularly in terms of the environmental impact. Although electric vehicles offer several advantages, there are certain restrictions that limit their usage. One of the significant issues is the uncertainty in their driving range. The driving range of EVs is closely related to their energy consumption, which is highly affected by exogenous and endogenous factors. Since those factors are unpredictable, uncertainty in EVs' energy consumption should be considered for efficient operation. This paper proposes a two-stage adaptive robust optimization framework for the electric vehicle routing problem. The objective is to minimize the worst-case energy consumption while guaranteeing that services are delivered at the appointed time windows without battery level deficiency. We postulate that EVs can be recharged on route, and the charging amount can be adjusted depending on the circumstances. A column-and-constraint generation based heuristic algorithm, which is coupled with variable neighbourhood search and alternating direction algorithm, is proposed to solve the resulting model. The computational results show the economic efficiency and robustness of the proposed model, and that there is a tradeoff between the total required energy and the risk of failing to satisfy all customers' demand.

## 1. Introduction

Over the last two decades, the transportation sector has rapidly grown. For instance, the number of registered vehicles in the US has increased by over 43% in the last 20 years (from 1990 to 2019) (see Statista, 2021). However, this rapid growth also brings some adverse effects, especially environmental problems. The United States Environmental Protection Agency (US EPA) reported that the transportation sector accounts for the most significant portion (29%) of the total greenhouse gas (GHG) emissions in the US for 2019 (US EPA, 2021). Also, Ge et al. (2020) reported that the transportation sector is one of the fastest-growing sources of GHG emissions, which has grown by 79% from 1990, and it is 16.2% of total global GHG emissions in 2019. Consequently, the interest in green vehicle routing has increased to overcome the environmental challenges facing the transportation sector.

In the recent decade, electric vehicles (EVs) have become the main interest of the transportation sector as a future mode of transportation because of their various benefits: cutting down on oil dependency, carbon dioxide ($CO_2$) emission reduction, less

* Corresponding author at: Ivey Business School of London, Canada.
*E-mail addresses:* jh5290@kaist.ac.kr (J. Jeong), bghaddar@ivey.ca, ghaddar@dtu.dk (B. Ghaddar), N.Zufferey@unige.ch (N. Zufferey), nathwani@uwaterloo.ca (J. Nathwani).

https://doi.org/10.1016/j.trc.2024.104529
Received 14 April 2023; Received in revised form 22 October 2023; Accepted 12 February 2024
Available online 1 March 2024

noise, and utilization of renewable energy (Bradley and Frank, 2009; Sioshansi and Denholm, 2009; Sundström and Binding, 2010; Yi and Bauer, 2017). Indeed, the number of EVs on the world's roads increased from 17,000 in 2010 to more than 10 million in 2020, and this number is rapidly growing worldwide (IEA, 2021). Additionally, many leading companies, such as UPS, FedEx, and Walmart, have deployed EV fleets in their operations (Winston, 2018). However, despite several benefits of EVs and their growing penetration, EVs still have critical issues limiting their usage. One issue is their limited driving range compared to conventional vehicles fuelled by gas or diesel. Other problems include the scarcity of the charging infrastructure and the long recharging time. Therefore, a more careful routing plan is needed to overcome EVs' limited driving range, especially for commercial EVs.

The driving range of EVs depends on the vehicle's battery capacity and its efficiency. Many factors relate to the vehicle's energy consumption efficiency, such as vehicle-, environmental- and driver-related factors, and several prediction models were proposed to forecast EV's energy consumption depending on those factors (Zhang et al., 2020; Basso et al., 2021). However, reliable forecasts of the EV's energy consumption may not be possible since many factors that impact an EV's energy consumption have a high degree of uncertainty or unpredictability. One of the major factors that affect EV's energy consumption efficiency is temperature. The temperature directly impacts the battery performance, but it also relates to the auxiliary heating and cooling of the vehicle. Cold or hot days make people use the air conditioning or heating system to cool or heat their vehicles respectively. The net effects of temperature and the resulting auxiliary power demand can decrease the EV's driving range by up to 40% compared to its maximum potential range (Yuksel and Michalek, 2015). Furthermore, even if the temperature can be precisely predicted, the EV's performance could be 32% higher or less than the expected driving range of that temperature depending on other factors, such as wind speed, rolling resistance, terrain, driver habits, trip length and start conditions (Yi and Bauer, 2017; GEOTAB, 2020). Therefore, to operate EVs efficiently, the uncertainty in EVs' energy consumption should be considered.

This paper aims to formulate and solve an optimization model for a practical delivery service system in which EVs are used for transporting products to customers, and all routes are guaranteed to withstand any realization of energy consumption uncertainties. To deal with uncertainty, we adopt an adaptive robust optimization framework (Ben-Tal et al., 2004) with time windows, partial recharge, and energy consumption rate uncertainty (AR-EVRPTWPR). It extends the electric vehicle routing problem with time windows and partial recharge (EVRPTWPR) proposed by Keskin and Çatay (2016) by considering the energy consumption rate uncertainty. The AR-EVRPTWPR is formulated as a two-stage adaptive robust problem and solved by means of a column-and-constraint generation framework (CCG) (Zeng and Zhao, 2013; Yu et al., 2022). Since the CCG decomposes the model into a master problem and subproblem, we apply the Variable Neighbourhood Search–Tabu Search (VNS-TS) metaheuristic (Schneider et al., 2014) and Alternating Direction (AD) algorithm (Konno, 1976) to solve the master problem and subproblem, respectively. The proposed solution method is a heuristic and is a modification of the classical CCG as it incorporates VNS-TS and AD. Additionally, the standard CCG solves the subproblem when the master problem finds an optimal solution. However, to accelerate the convergence, the proposed approach solves the subproblem whenever VNS-TS finds a robust feasible solution to the master problem. Once a robust feasible solution for the current master problem is found, AD solves the subproblem to detect if this current solution violates any scenario not considered in the master problem. Decision variables and constraints are generated for the detected violated scenario from the subproblem and added to the master problem and as a result the VNS cost function is adjusted to take the violated scenario into account. The proposed method is applied to test instances of Schneider et al. (2014) to show the performance of the approach. Thus the contribution of this paper is three folds: (1) formulating an adaptive robust EVRPTWPR with energy consumption rate uncertainty, (2) using a customized CCG framework to solve the proposed problem, where the VNS-TS approach is used to solve the multi-scenario EVRPTWPR master problem and an AD is used to solve the subproblem. As VNS-TS has not been used before to solve multiple scenarios for this problem, we propose a new cost function to account for the multiple constraints related to the different scenarios. Additionally, since solving the VNS-TS at each iteration is expensive we adopt a "warm starting" strategy where the VNS-TS continues from the previous solution to find a new robust feasible solution once a new scenario is added, finally (3) presenting computational results and analysis to compare the deterministic and the ARO approach.

The remainder of this paper is organized as follows. Section 2 presents a literature review of related work. Section 3 provides the mathematical formulation of AR-EVRPTWPR. The proposed solution methods are presented in Section 4. In Section 5, computational experiments are conducted for the proposed AR-EVRPTWPR. Finally, conclusions and future research directions are drawn in Section 6.

## 2. Literature review

Since 1959, when (Dantzig and Ramser, 1959) first proposed the vehicle routing problem (VRP), VRP has been extensively studied for its variants and solution methods (Eksioglu et al., 2009; Toth and Vigo, 2014; Braekers et al., 2016). The objective of VRP is to find a set of routes for a fleet of vehicles that minimizes the total travel distances while it starts from the depot, visits a given set of customers, and returns to the depot. Recently, the green vehicle routing problem, a variation of VRP, has been widely studied due to the negative effects of transportation on the environment. A comprehensive review of green vehicle routing problems can be found in Demir et al. (2014), Lin et al. (2014), Bektaş et al. (2019).

The electric vehicle routing problem (EVRP) is a variation of the VRP where EVs are integrated into the distribution operations. Conrad and Figliozzi (2011) propose a capacitated recharging VRP with customer time windows. Schneider et al. (2014) consider an E-VRPTW, an EVRP with time windows and recharging stations. EVs' batteries can be recharged at recharging stations, and only full recharge is allowed. The E-VRPTW was extended to consider partial recharge by Felipe et al. (2014), Keskin and Çatay (2016), and Schiffer and Walther (2017). Hiermann et al. (2019) considered a fleet mix with several types of vehicles. Cortés-Murcia et al. (2019) regarded the recharging time as an idle time and allowed for servicing the customers by walking from the recharging

**Table 1**
Summary on the literature of electric vehicle routing problem with recharging stations.

| Paper | Time windows | Recharging strategy | Recharging function | Source of uncertainty | Modelling approach |
|---|---|---|---|---|---|
| Conrad and Figliozzi (2011) | ✓ | Fixed (parameterized) | Fixed constant | ✗ | Deterministic Mixed Integer Nonlinear Programming model |
| Felipe et al. (2014) | ✗ | Partial & multiple technologies | Linear function | ✗ | Deterministic MILP model |
| Schneider et al. (2014) | ✓ | Full | Linear function | ✗ | Deterministic MILP model |
| Keskin and Çatay (2016) | ✓ | Partial | Linear function | ✗ | Deterministic MILP model |
| Montoya et al. (2017) | ✗ | Partial | Piecewise linear function | ✗ | Deterministic MILP model |
| Schiffer and Walther (2017) | ✓ | Partial | Linear function | ✗ | Deterministic MILP model |
| Cortés-Murcia et al. (2019) | ✗ | Partial | Linear function | ✗ | Deterministic MILP model |
| Froger et al. (2019) | ✓ | Partial & multiple technologies | Piecewise linear function | ✗ | Deterministic MILP model |
| Hiermann et al. (2019) | ✗ | Partial & multiple technologies | Piecewise linear function | ✗ | Deterministic MILP model |
| Pelletier et al. (2019) | ✗ | Partial | Linear function | Energy consumption | Robust optimization model |
| Basso et al. (2021) | ✗ | Partial | Linear function | Energy consumption | Two-stage model with chance constraints |
| Lee (2021) | ✗ | Partial | Non-decreasing Concave function | ✗ | Deterministic Mixed Integer Nonlinear Programming model |
| Basso et al. (2022) | ✓ | Full | Linear function | Customer requests & Energy consumption | Markov Decision Process Model |
| Froger et al. (2022) | ✓ | Partial & Multiple speeds | Piecewise linear function | ✗ | Deterministic MILP model |
| Zang et al. (2022) | ✓ | Partial | Piecewise linear function | ✗ | Deterministic MILP |
| Current work | ✓ | Partial | Linear function | Energy consumption | Two-stage adaptive robust optimization model |

station while the EV is recharging. The recent trend in EVRP considers a nonlinear recharging process. The battery recharging rate varies depending on the remaining battery capacity. Thus, the recharging function is represented as a nonlinear function (Pelletier et al., 2017). Typically, the nonlinearity is approximated using a piecewise linear charging function (Froger et al., 2022, 2019; Montoya et al., 2017; Zang et al., 2022). Other work directly considers the nonlinear recharging function postulated as a concave and non-decreasing function (Lee, 2021).

The above studies consider deterministic parameters, i.e., the expected or average value of energy consumption, travel time, demand, and recharging time. Thus, a solution obtained from a deterministic EVRP would be very vulnerable to variations in the parameters. Some stochastic variants of EVRP have been proposed to deal with the uncertainty in EVRP, such as considering stochastic waiting times at recharging stations (Keskin et al., 2019, 2021), stochastic customer requests, and stochastic energy consumption (Basso et al., 2022). Also, a robust optimization model is proposed by Pelletier et al. (2019) to take into account energy consumption uncertainty in capacitated EVRP. Basso et al. (2021) applied a probabilistic Bayesian machine learning approach to predict energy consumption and modelled the problem as an EVRP with chance-constrained partial recharging.

Adaptive (or adjustable) robust optimization (ARO) is a branch of robust optimization (RO), which recently has an increased range of applications (Yanıkoğlu et al., 2019). ARO allows a subset of decision variables to adapt against uncertainty scenarios in the uncertainty set. Comprehensive studies of the ARO approach can be found in various applications including power system operation (Bertsimas et al., 2012; Wang et al., 2013; Lorca and Sun, 2014). Also, ARO has been applied for inventory routing problems (Agra et al., 2018). To the best of our knowledge, there has not been any research considering energy consumption uncertainty in EVRP using an ARO approach. In the context of EVRP, energy consumption uncertainty was considered in Pelletier et al. (2019), Basso et al. (2021), and Basso et al. (2022). Pelletier et al. (2019) adopt the RO approach that only considers the worst energy consumption. Basso et al. (2021) account for chance constraints with energy consumption prediction through machine learning techniques. Additionally, Basso et al. (2022) consider stochastic customer requests and stochastic energy consumption for the dynamic stochastic EVRP (DS-EVRP), and the DS-EVRP is modelled as a Markov Decision Process. Table 1 summarizes the related works on EVRP with recharging stations and highlights the different assumptions used (presence of time window constraints, use of fixed or partial charging, and type of recharging function).

The RO approach usually provides a conservative solution, and the solution quality of the chance constraints approach highly depends on which distribution function is used. However, ARO generally provides a less conservative solution than the classical RO approach because ARO separates decision variables into two groups: here-and-now and wait-and-see decisions. Here-and-now decisions should be determined before the uncertainty realization, but wait-and-see decisions can adapt to the uncertainty realization. This ARO's characteristic is similar to the nature of the EV routing problem under consideration. Each EV's route should be planned at least a day ahead to have the schedule of the EV delivery fleet, but the recharging amount can be decided while on route based on the operating situation. Therefore, ARO approach is more suitable to consider uncertainties in routing problems. Also, the solution quality of the ARO approach does not depend on the distribution function like the chance-constrained approach. Instead, the ARO approach requires more simple statistics, such as mean and variance. Thus, the ARO approach does not depend on estimating the precise distribution which might not be possible in some applications.

The main contributions of this paper are twofold. The first is to introduce and formulate an adaptive robust optimization model of a delivery routing problem where a fleet of EVs needs to visit a given set of customers regardless of any realization of energy consumption scenario within the uncertainty set. The second is to solve the resulting two-stage adaptive robust model efficiently and for that we propose a decomposition solution framework based on CCG approach. Additionally, we show the performance of the proposed methodology on a set of test instances taken from the literature.

## 3. EVRPTWPR formulations

In this section, we describe the motivation for developing an adaptive robust EVRPTWPR with energy consumption rate uncertainty and then present its mathematical formulation. We first describe the deterministic EVRPTWPR model and then formulate the adaptive robust EVRPTWPR with energy consumption rate uncertainty (AR-EVRPTWPR). Both models are mixed-integer programming problems. A brief explanation of adopting the adaptive robust optimization is provided.

### 3.1. Deterministic EVRPTWPR formulation

We use a similar representation of the deterministic EVRPTWPR model as the one presented in Keskin and Çatay (2016) and follow a similar notation (as shown in Table 2). The EVRPTWPR model in Keskin and Çatay (2016) minimizes the total travel distance while satisfying all customers' demands within the time windows. The EVs' energy consumption is proportional to the travel distance. Linear recharging function is considered and partial recharge is allowed at recharging stations; all recharging stations are assumed to be homogeneous. We note that the battery recharging function is assumed to be a linear function to avoid challenges that could arise from the nonlinear recharging function once embedded in an ARO framework. In this work, we deal with a different objective function since we consider an energy consumption rate uncertainty. Thus instead of minimizing the total travel distance, we propose to minimize the total amount of recharging en routes. Since we consider the energy consumption rate as the uncertain parameter, minimizing the consumed energy is more appropriate than minimizing the total travel distance. For example, there could be a route providing a shorter travel distance but requiring more energy. We note that if there is no energy consumption rate uncertainty and under the same assumptions in Keskin and Çatay (2016), the optimal solution of our deterministic model provides the same total travel distance compared to the EVRPTWPR model with the objective function of minimizing the total travel distance. It is evident as the recharging amount is directly related to the travel distance for the deterministic model. Also, we note that we here use a three-index model for the ease of implementing the solution methods introduced in Section 4. Thus, for the deterministic model, we follow a similar three-index model formulation to the one used by Lin et al. (2021). The deterministic model with time window constraints and partial recharging is formulated as the following mixed-integer linear programming model:

$$\min \quad \sum_{k\in K}\sum_{i\in F_0} p_{ik} \tag{1a}$$

$$\text{s.t.} \quad \sum_{k\in K}\sum_{j\in V_{N+1}, i\neq j} x_{ijk} = 1 \qquad \forall i \in P \tag{1b}$$

$$\sum_{i\in V_0, i\neq j} x_{ijk} - \sum_{i\in V_{N+1}, i\neq j} x_{jik} = 0 \qquad \forall j \in V, k \in K \tag{1c}$$

$$\sum_{j\in V_{N+1}} x_{0,j,k} \leq 1, \qquad \forall k \in K \tag{1d}$$

$$\tau_{ik} + (t_{ij} + s_i)x_{ijk} - l_0(1 - x_{ijk}) \leq \tau_{jk} \qquad \forall i \in P_0, j \in V_{N+1}, i \neq j, k \in K \tag{1e}$$

$$\tau_{ik} + t_{ij}x_{ijk} + g_i \cdot p_{ik} - (l_0 + gB)(1 - x_{ijk}) \leq \tau_{jk} \qquad \forall i \in F, j \in V_{N+1}, i \neq j, k \in K \tag{1f}$$

$$e_j \leq \tau_{jk} \leq l_j \qquad \forall j \in V_{0,N+1}, k \in K \tag{1g}$$

$$0 \leq u_{jk} \leq u_{ik} - q_i \cdot x_{ijk} + C(1 - x_{ijk}) \qquad \forall i \in V_0, j \in V_{N+1}, i \neq j, k \in K \tag{1h}$$

$$0 \leq u_{0k} \leq C \qquad \forall k \in K \tag{1i}$$

$$0 \leq y_{jk} \leq y_{ik} - (h_{ij} \cdot d_{ij})x_{ijk} + B(1 - x_{ijk}) \qquad \forall i \in P, j \in V_{N+1}, i \neq j, k \in K \tag{1j}$$

$$0 \leq y_{jk} \leq y_{ik} + p_{ik} - (h_{ij} \cdot d_{ij})x_{ijk} + B(1 - x_{ijk}) \qquad \forall i \in F_0, j \in V_{N+1}, i \neq j, k \in K \tag{1k}$$

$$y_{ik} + p_{ik} \leq B \qquad \forall i \in F_0, k \in K \tag{1l}$$

$$x_{ijk} \in \{0,1\} \qquad \forall i \in V_0, j \in V_{N+1}, i \neq j, k \in K \tag{1m}$$

$$p_{ik} \geq 0 \qquad \forall i \in F_0, k \in K, \tag{1n}$$

where $R$, $F$, and $K$ denote the sets of customers, recharge stations, and vehicles, respectively, and $V := R \cup F, V_0 := V \cup \{0\}, V_{N+1} := V \cup \{N+1\}$, and $F_0 := F \cup \{0\}$ where 0 and $N+1$ denote the initial depot and the end depot, respectively. We note that EVs are allowed to re-visit recharge stations. Thus, the set $F$ is defined as $F = \{N+2, \ldots, N+1+NF, N+2+NF, \ldots, N+1+\nu+NF\}$, where $NF$ and $\nu$ are the number of recharging stations and the number of allowed re-visits, respectively. Decision variable $x_{ijk}$ is the binary decision of travel of arc $(i,j)$ by vehicle $k$, $u_{jk}$ is the load level decision of vehicle $k$ at vertex $j$, $\tau_{jk}$ and $y_{kj}$ specify the service start time and battery level when the vehicle $k$ arrives at vertex $j$, respectively, and $p_{jk}$ is the battery recharging amount decision of the vehicle $k$ at the vertex $j$. Parameters $C, B$, and $g_i$ are the load capacity, battery capacity, and recharging rate, respectively, and $h_{ij}$ is the energy consumption rate on arc $(i,j)$. Also, $e_j$ and $l_j$ are the earliest and latest service start time at vertex $j$. The details of sets, variables, and parameters used in this paper are summarized in Table 2. The objective (1a) minimizes the amount of the recharging en routes. Constraints (1b) ensure that all customers are satisfied by one single EV. Constraints (1c) correspond to the flow conservation for each vertex, where the number of incoming and outgoing flows should be the same. We add constraint (1d) to enforce that each vehicle should be dispatched at most once. Constraints (1e) and (1f) enforce arcs' time feasibility leaving from a vertex in $R_0$ and $F$, respectively. We note that a linear recharging process is assumed in (1f). Constraints (1g) ensure the time windows of each vertex. Constraints (1h) and (1i) enforce the demand fulfilment of all customers, and load level should be nonnegative and cannot exceed the vehicle's capacity. Constraints (1j) and (1k) enforce that the vehicle's battery charge level is always non-negative. Constraints (1l) state that the vehicle's battery charge level departing vertex $j$ should be larger than its battery charge level when it arrives and cannot exceed its battery capacity.

### 3.2. AR-EVRPTWPR formulation

In this section, we propose an ARO model for EVRPTWPR with energy consumption rate uncertainty. We assume that energy consumption rate realization would be different depending on arc $(i,j)$. Thus $h_{ij}$, which is the energy consumption rate on arc $(i,j)$, is an uncertain parameter in the proposed model.

The motivation for adopting the ARO approach is related to the nature of recharging decisions. First, the drivers usually decide whether to recharge or not, depending on how much of the vehicle's driving range remains. Thus, the recharging decision can be adjustable depending on the circumstance. Second, as highlighted in Section 1, many factors can increase or decrease the EVs' energy consumption rate. In practice, it is difficult to forecast in advance which factors will affect the EVs' energy consumption rate realization, and a plan for the recharging station visit could be useless. Therefore, for efficient EV fleet operation, the recharging decision should be regarded as adaptive on uncertainty realization and not scheduled in advance. Since the classical RO approach deals with the uncertainty of data by finding a robust solution immunized against all possible scenarios in a predefined set (Ben-Tal et al., 2004; Bertsimas et al., 2011), it is not appropriate to the nature of the recharging decisions in EVRP. On the other hand, the ARO approach allows some decision variables to be varied to deal with the different uncertainty realizations. Specifically, in the ARO approach, decision variables are categorized into two groups, non-adaptive and adaptive decision variables. The non-adaptive decisions are assumed to be decided before any uncertainty realization and should be feasible for all possible uncertainties, the same as the classical RO approach. However, adaptive decisions are made after the uncertainty realization. For these reasons, we apply the adaptive robust optimization approach for the EVRPTWPR in our work.

In this paper, we focus on the AR-EVRPTWPR. Therefore, instead of presenting the RO-EVRPTWPR, we refer the reader to Gounaris et al. (2013) and Munari et al. (2019). AR-EVRPTWPR is formulated as a two-stage adaptive robust model. To apply a two-stage ARO approach to the EVRPTWPR with energy consumption rate uncertainty, the decision variables should be categorized into two groups, which are *non-adaptive* (or *here-and-now*) and *adaptive* (or *wait-and-see*) variables. The former non-adaptive decisions should be made before uncertainty realization. However, the latter adaptive decisions are made after the uncertainty realization. The three-index EVRPTWPR has five types of decision variables: $x_{ijk}, \tau_{ik}, u_{ik}, y_{ik}$, and $p_{ik}$. Among these variables, $x_{ijk}$ and $u_{ik}$ are clearly non-adaptive variables. The route for each vehicle should be decided before the trip, and energy consumption rate uncertainty is not considered. There are several reasons for also including the charging station visit in the first stage, one is methodological and the other is related to the implementation of the model in practice. On the methodological side, if part of EVs' routes is assumed to be adaptive, then the model would contain binary adaptive decisions which introduce a substantial computational difficulty. Another point is if only the sequences of customers are fixed, it can increase the total travel distance in case of visiting charging stations was a decision in the second stage. Also in practice, drivers prefer to have a fixed route for the next day, thus if they do not know the charging stations they need to charge at, the route is not known in advance which might be a problem from an operational practical side.

Variables $p_{ik}$ are adaptive variables as they are impacted by the uncertainty of the energy consumption rate. We note that the other two decision variables $\tau_{ik}$ and $y_{ik}$ are determined via the energy consumption realization. Therefore, they are adaptive variables. Adaptive decision variables are represented as a function of the uncertain parameter $\boldsymbol{h}$, where $\boldsymbol{h}$ is the vector of energy consumption rate at all arcs. Therefore, adaptive variables $p_{ik}$, $\tau_{ik}$, and $y_{ik}$ are represented as $p_{ik}(\boldsymbol{h})$, $\tau_{ik}(\boldsymbol{h})$, and $y_{ik}(\boldsymbol{h})$, respectively. Since we consider a two-stage AR-EVRPTWPR, we postulate that the realizations of the uncertain energy consumption rates are

**Table 2**
Summary of notation.

| | |
|---|---|
| **Sets** | |
| $0, N+1$ | Initial depot and end depot |
| $P$ | Set of customer vertices $P := \{1, 2, \dots, N\}$ |
| $P_0$ | $P_0 := P \cup \{0\}$ |
| $F$ | Set of recharge station vertices |
| $V$ | Set of customers and recharge stations vertices $V := P \cup F$ |
| $V_0$ | $V_0 := V \cup \{0\}$ |
| $V_{N+1}$ | $V_{N+1} := V \cup \{N+1\}$ |
| $V_{0,N+1}$ | $V_{0,N+1} := V \cup \{0, N+1\}$ |
| $F_0$ | $F_0 := F \cup \{0\}$ |
| $\mathcal{A}$ | Set of arcs $\mathcal{A} := \{(i,j) \mid i \in V_0, j \in V_{N+1}, i \neq j\}$ |
| $K$ | Set of homogeneous vehicles |
| $\mathcal{U}$ | Set of possible energy consumption rate scenarios |
| $\mathcal{R}$ | Set of routes. For convenience, we call "route $\mathcal{R}$" instead of "the set of routes $\mathcal{R}$" |
| **Variables** | |
| $x_{ijk}$ | Binary decision variable for the arc $(i,j)$ travelling by vehicle $k$. |
| $u_{jk}$ | Nonnegative continuous decision variable for the remaining load level when the vehicle $k$ arrives at vertex $j$ |
| $\tau_{jk}$ | Continuous decision variable for the service start time of the vehicle $k$ at vertex $j$ |
| $y_{jk}$ | Nonnegative continuous decision variable for battery charge level when the vehicle $k$ arrives at vertex $j$ |
| $p_{jk}$ | Nonnegative continuous decision variable for battery recharging amount of the vehicle $k$ at vertex $j$ |
| **Parameters** | |
| $d_{ij}$ | Distance of arc $(i,j)$ |
| $t_{ij}$ | Travel time of arc $(i,j)$ |
| $q_j$ | Demand of customer $j$ |
| $s_j$ | service time of customer $j$ |
| $e_j, l_j$ | Earliest and latest start time of customer $j$ |
| $C$ | Vehicle capacity |
| $B$ | Vehicle battery capacity |
| $g_i$ | Recharging rate at station $i$ |
| $h_{ij}$ | Energy consumption rate on arc $(i,j)$ |
| $NF$ | Number of recharge stations |
| $\nu$ | Number of allowed re-visits |

simultaneously revealed. This assumption could be reasonable since some exogenous factors, such as temperature, could be estimated reasonably well at the beginning of the day. We note that minimizing the worst energy recharging amount is equivalent to minimizing the worst energy consumption value. Based on this observation, we formulate the AR-EVRPTWPR as follows:

$$\min \quad \max_{\boldsymbol{h} \in \mathcal{U}} \sum_{k \in K} \sum_{i \in F_0} p_{ik}(\boldsymbol{h}) \tag{2a}$$

$$\text{s.t.} \quad \sum_{k \in K} \sum_{j \in V_{N+1} \setminus \{i\}} x_{ijk} = 1 \qquad \forall i \in P \tag{2b}$$

$$\sum_{i \in V_0 \setminus \{j\}} x_{ijk} - \sum_{i \in V_{N+1} \setminus \{j\}} x_{jik} = 0 \qquad \forall j \in V, k \in K \tag{2c}$$

$$\sum_{j \in V_{N+1}} x_{0,j,k} \leq 1, \qquad \forall k \in K \tag{2d}$$

$$\tau_{ik}(\boldsymbol{h}) + (t_{ij} + s_i) x_{ijk} - l_0(1 - x_{ijk}) \leq \tau_{jk}(\boldsymbol{h}) \qquad \forall \boldsymbol{h} \in \mathcal{U}, i \in P_0, j \in V_{N+1}, i \neq j, k \in K \tag{2e}$$

$$\tau_{ik}(\boldsymbol{h}) + t_{ij} x_{ijk} + g_i \cdot p_{ik}(\boldsymbol{h}) - (l_0 + gB)(1 - x_{ijk}) \leq \tau_{jk}(\boldsymbol{h}) \qquad \forall \boldsymbol{h} \in \mathcal{U}, i \in F, j \in V_{N+1}, i \neq j, k \in K \tag{2f}$$

$$e_j \leq \tau_{jk}(\boldsymbol{h}) \leq l_j \qquad \forall \boldsymbol{h} \in \mathcal{U}, j \in V_{0,N+1}, k \in K \tag{2g}$$

$$0 \leq u_{jk} \leq u_{ik} - q_i \cdot x_{ijk} + C(1 - x_{ijk}) \qquad \forall i \in V_0, j \in V_{N+1}, i \neq j, k \in K \tag{2h}$$

$$0 \leq u_{0k} \leq C \qquad \forall k \in K \tag{2i}$$

$$0 \leq y_{jk}(\boldsymbol{h}) \leq y_{ik}(\boldsymbol{h}) - (h_{ij} \cdot d_{ij}) x_{ijk} + B(1 - x_{ijk}) \qquad \forall \boldsymbol{h} \in \mathcal{U}, i \in P, j \in V_{N+1}, i \neq j, k \in K \tag{2j}$$

$$0 \leq y_{jk}(\boldsymbol{h}) \leq y_{ik}(\boldsymbol{h}) + p_{ik}(\boldsymbol{h}) - (h_{ij} \cdot d_{ij}) x_{ijk} + B(1 - x_{ijk}) \qquad \forall \boldsymbol{h} \in \mathcal{U}, i \in F_0, j \in V_{N+1}, i \neq j, k \in K \tag{2k}$$

$$0 \le y_{ik}(\boldsymbol{h}) + p_{ik}(\boldsymbol{h}) \le B \qquad \forall \boldsymbol{h} \in \mathcal{U}, i \in F_0, k \in K \tag{2l}$$

$$0 \le p_{ik}(\boldsymbol{h}) \qquad \forall \boldsymbol{h} \in \mathcal{U}, i \in V_{0,N+1}, k \in K \tag{2m}$$

$$x_{ijk} \in \{0,1\} \qquad \forall i \in V_0, j \in V_{N+1}, i \ne j, k \in K, \tag{2n}$$

where $\tau(\boldsymbol{h}), y(\boldsymbol{h}), p(\boldsymbol{h})$ denote the functional form of the adaptive decision variables for energy consumption rate scenario $\boldsymbol{h}$. In other words, $\tau, y$, and $p$ are determined for the energy consumption rate scenarios $\boldsymbol{h}$. The objective (2a) minimizes the worst recharging amount for all energy consumption rate realization $\boldsymbol{h} \in \mathcal{U}$. Constraints with only non-adaptive decision variables, such as (2b)–(2c) and (2h)–(2i), are the same as the constraints (1b)–(1e) and (1h)–(1i), respectively. All of the constraints that contain adaptive decision variables become a robust constraint, such as (2e)–(2g) and (2j)–(2m). Constraints (2e)–(2g) and (2j)–(2m) enforce arcs' time feasibility, time window, non-negative battery charge level, and bounds of the battery charge level for any energy consumption rate realization $\boldsymbol{h} \in \mathcal{U}$. For the uncertainty set $\mathcal{U}$, we consider the following budget uncertainty set:

$$\mathcal{U} := \left\{ \boldsymbol{h} \in \mathbb{R}^{|\mathcal{A}|} : \sum_{a \in \mathcal{A}} \frac{|h_a - \bar{h}_a|}{\hat{h}_a} \le \Gamma, h_a \in [\bar{h}_a - \hat{h}_a, \bar{h}_a + \hat{h}_a], \forall a \in \mathcal{A} \right\}, \tag{3}$$

where $\mathcal{A} := \{(i,j) : i \in V_{0,N+1}, j \in V_{0,N+1}, i \ne j\}$ is the set of arcs, $\bar{h}_a$ is the expected energy consumption rate of arc $a$, $\hat{h}_a := 0.1 \times \bar{h}_a$, and $\Gamma$ is the "budget of uncertainty" (Bertsimas et al., 2012). The uncertainty set (3) assumes that the energy consumption rate is realized within a certain range. The cardinality constraint limits the total deviation of uncertain energy consumption rates from their expected values.

Compared to the deterministic model (1), the model (2) is still a mixed-integer programming problem. However, model (2) has a min–max objective function and adaptive decision variables are represented in a function of uncertain parameters. The min–max objective function cannot be handled directly, and the expression of adaptive decision variables is closely related to the tractability of the model (2). Thus, the presented model (2) is hard to solve using standard methods. In the following section, we introduce a solution framework to solve the proposed model given in (2).

## 4. Solution methods

The AR-EVRPTWPR formulation presented in problem (2), depicts a two-stage structure. The first-stage variables are non-adjustable and the second-stage variables are adjustable based on the first stage. In particular, the first stage finds the route and load level decision immunized against all possible uncertainty realization $\boldsymbol{h} \in \mathcal{U}$. In the second stage, the decision should be adaptive to any uncertainty realization $\boldsymbol{h} \in \mathcal{U}$, and provide a minimum worst-case cost. To simplify the notation, we present the compact matrix form of problem (2) as follows with matrices and vectors shown in bold:

$$\min_{\boldsymbol{x}, \boldsymbol{y}(\cdot)} \max_{\boldsymbol{h} \in \mathcal{U}} \ \boldsymbol{b}^\top \boldsymbol{y}(\boldsymbol{h}) \tag{4a}$$

$$\text{s.t.} \quad \boldsymbol{A}\boldsymbol{x} \le \boldsymbol{d} \tag{4b}$$

$$\boldsymbol{F}\boldsymbol{y}(\boldsymbol{h}) \le \boldsymbol{f} \qquad \forall \boldsymbol{h} \in \mathcal{U} \tag{4c}$$

$$\boldsymbol{G}(\boldsymbol{h})\boldsymbol{x} + \boldsymbol{H}\boldsymbol{y}(\boldsymbol{h}) \le \boldsymbol{g} \qquad \forall \boldsymbol{h} \in \mathcal{U}, \tag{4d}$$

where the vector $\boldsymbol{x}$ is the vector of non-adaptive decision variables, including the route and load level decisions. The vector $\boldsymbol{y}$ is the vector of adaptive decision variables, including the arrival time, battery energy level, and battery charge level decisions. The functional form $\boldsymbol{y}(\boldsymbol{h})$ represents that $\boldsymbol{y}$ is fully adaptive to any uncertainty realization $\boldsymbol{h} \in \mathcal{U}$. Constraint (4b) includes route-related constraints (2b)–(2d) and vehicle's cargo level-related constraints (2h) and (2i). Constraint (4c) contains (2g), (2l), and (2m). Constraint (4d) couples the non-adaptive and adaptive decisions, including (2e), (2f), (2j), and (2k).

We note that the energy consumption rate uncertainty in AR-EVRPTWPR is column-wise, so robust constraints cannot be dualized to obtain a robust counterpart and thus obtain a single-stage. Several solution methods were proposed to solve this type of problem, such as Benders decomposition with cutting planes algorithm (Bertsimas et al., 2012; Wang et al., 2013), linear decision rule approximation (Ben-Tal et al., 2004, 2005; Dehghan et al., 2017), and column-and-constraint generation method (Zeng and Zhao, 2013). Using the linear decision rule, e.g., an affine policy approximation for the adaptive decision variables, is not suitable for the AR-EVRPTWPR in this case because it increases the number of decision variables and the resulting problem easily becomes intractable. The remaining potential solution methods for the AR-EVRPTWPR are the Benders decomposition approach and the column-and-constraint generation method. Both methods are very similar since they decompose the problem into a master and subproblem, and iteratively solve them until the master problem provides a robust optimal solution for all uncertainties. The only difference between them is the type of constraints that are added to the master problem. In the column-and-constraint generation (CCG) method, a copy of the variables and the constraints of the original model are added to the master problem. On the other hand, single or multi-Benders cuts are added to the master problem in the Benders decomposition approach. For the AR-EVRPTWPR, the master problem of the CCG method can be formulated as an EVRPTWPR with multiple energy consumption rate scenarios. The resulting formulation has the advantage of evaluating time window and battery capacity violations using existing methods such as the ones presented by Schiffer and Walther (2018) and Cortés-Murcia et al. (2019). Thus, in this work we adopt a similar approach to the CCG introduced in Zeng and Zhao (2013) to solve the AR-EVRPTWPR.

### 4.1. Column-and-constraint generation framework

We first introduce the master problem and subproblem of the CCG method. Formulation (4) is equivalent to the following model:

$$\min_{\boldsymbol{x},\eta} \quad \eta \tag{5a}$$

$$\text{s.t.} \quad \boldsymbol{A}\boldsymbol{x} \le \boldsymbol{d} \tag{5b}$$

$$\eta \ge \min_{\boldsymbol{y}\in\boldsymbol{\Omega}(\boldsymbol{x},\boldsymbol{h})} \boldsymbol{b}^\top \boldsymbol{y} \qquad \forall \boldsymbol{h} \in \mathcal{U}, \tag{5c}$$

where $\boldsymbol{\Omega}(\boldsymbol{x},\boldsymbol{h}) = \{\boldsymbol{y} : \boldsymbol{F}\boldsymbol{y} \le \boldsymbol{f}, \boldsymbol{G}(\boldsymbol{h})\boldsymbol{x} + \boldsymbol{H}\boldsymbol{y} \le \boldsymbol{g}\}$ is the set of feasible arrival time, load level, battery level, and battery charge level for a given fixed route $\boldsymbol{x}$ and an energy consumption $\boldsymbol{h}$. Since the uncertainty set $\mathcal{U}$ is a polytope, $\mathcal{U}$ in constraint (5c) can be replaced by the set of its extreme points, denoted by ext($\mathcal{U}$) (Bertsimas et al., 2012; Zeng and Zhao, 2013). We note that the set ext($\mathcal{U}$) has a finite number of energy consumption rate scenarios. Therefore, problem (5) can be written as follows:

$$\min_{\boldsymbol{x},\eta,\boldsymbol{y}^s} \quad \eta \tag{6a}$$

$$\text{s.t.} \quad \boldsymbol{A}\boldsymbol{x} \le \boldsymbol{d} \tag{6b}$$

$$\eta \ge \boldsymbol{b}^\top \boldsymbol{y}^s \qquad \forall s \in I(\text{ext}(\mathcal{U})) \tag{6c}$$

$$\boldsymbol{y}^s \in \boldsymbol{\Omega}(\boldsymbol{x},\boldsymbol{h}^s) \qquad \forall s \in I(\text{ext}(\mathcal{U})), \tag{6d}$$

where $I(\text{ext}(\mathcal{U}))$ is the index set of scenarios in the set ext($\mathcal{U}$), $\boldsymbol{y}^s$ is the decision variable $\boldsymbol{y}$ at scenario $s$, and $\boldsymbol{h}^s$ is the energy consumption scenario of $\boldsymbol{h}$ for the $s$th scenario in the set ext($\mathcal{U}$). We note that variable $\boldsymbol{y}$ and the associated constraint set are repeated as much as the number of scenarios in the set ext($\mathcal{U}$). The number of constraints and variables in (6) is around $|\text{ext}(\mathcal{U})|$ times that of the deterministic EVRPTWPR model, and is thus intractable. To obtain a tractable way to solve this problem, we adopt an iterative approach where CCG starts from the relaxed master problem (RMP), which has a subset of the set ext($\mathcal{U}$) in problem (6). This RMP can be defined as the EVRPTWPR with multiple scenarios of the energy consumption rate. We refer to this problem as [RMP($\bar{\mathcal{U}}$)], where $\bar{\mathcal{U}} \subseteq \text{ext}(\mathcal{U})$. Let $(\boldsymbol{x}^*, \eta^*)$ be the optimal solution of the current [RMP($\bar{\mathcal{U}}$)]. The details of the solution method for solving the [RMP($\bar{\mathcal{U}}$)] are described in Sections 4.2 and 4.4.

The next step identifies the worst-case scenario $\tilde{\boldsymbol{h}}$ that defines the largest objective function value of the subproblem with a fixed $\boldsymbol{x}^*$ and is not in $\bar{\mathcal{U}}$. The subproblem, [SP($\boldsymbol{x}^*$)], is defined by fixing the non-adaptive decision $\boldsymbol{x}$. Thus, [SP($\boldsymbol{x}^*$)] is stated as follows:

$$\max_{\boldsymbol{h}\in\mathcal{U}} \min_{\boldsymbol{y}} \quad \boldsymbol{b}^\top \boldsymbol{y} \tag{7a}$$

$$\text{s.t.} \quad \boldsymbol{F}\boldsymbol{y} \le \boldsymbol{f} \tag{7b}$$

$$\boldsymbol{H}\boldsymbol{y} \le \boldsymbol{g} - \boldsymbol{G}(\boldsymbol{h})\boldsymbol{x}^* \qquad \forall \boldsymbol{h} \in \mathcal{U}. \tag{7c}$$

We note that $\boldsymbol{h} \in \mathcal{U}$ is used in problem (7) instead of $\boldsymbol{h} \in \text{ext}(\mathcal{U})$ since the optimal solution $\boldsymbol{h}^*$ is an extreme point of the polyhedron $\mathcal{U}$ (Zeng and Zhao, 2013). The subproblem [SP($\boldsymbol{x}^*$)] detects the worst-case scenario $\tilde{\boldsymbol{h}}$ that defines the largest amount of consumed energy for a fixed $\boldsymbol{x}^*$. There could be a scenario that makes the current solution $\boldsymbol{x}^*$ infeasible. To guarantee the feasibility of the subproblem (7), slack variables could be added to constraints (7b) and (7c). Then, the corresponding objective terms of slack variables should be added to the objective function (7a). The details of a model including the slack variables and the proposed solution approach are described in Section 4.3. If the optimal value of the subproblem (7), $\zeta^*$, is bigger than $\eta^*$, then the detected scenario $\tilde{\boldsymbol{h}}$ is added to the set $\bar{\mathcal{U}}$, and new variables and constraints corresponding to $\tilde{\boldsymbol{h}}$ are generated and added to [RMP($\bar{\mathcal{U}}$)]. The size of the RMP grows with every iteration. The overall CCG framework for solving AR-EVRPTWPR is summarized in Algorithm 1. We note that the Algorithm 1 terminates only when $\zeta^* - \eta^* < \delta$. The convergence tolerance $\delta$ should be nonnegative and sufficiently small since it can impact the solution quality. For the computational results, we set $\delta$ to 0.001. In the following sections, we illustrate solution methods for [RMP($\bar{\mathcal{U}}$)] and [SP($\boldsymbol{x}^*$)]. Due to their computational complexities, both models are solved using heuristic methods and the performance of the proposed solution framework is demonstrated in Section 5.

**Algorithm 1** Column-and-Constraint Generation Framework

```
1: Ū ← {h̃}
2: x ← InitialSolution(Ū)
3: RobustFeasibility ← False
4: while –RobustFeasibility do
5:     x*, η* ← [RMP(Ū)]
6:     ζ*, h̃ ← [SP(x*)]
7:     if ζ* − η* ≥ δ then
8:         Ū ← Ū ∪ {h̃}
9:     else
10:        RobustFeasibility ← True
```

### 4.2. Solution methods for the master problem

As we have seen in the previous section, [RMP($\bar{\mathcal{U}}$)] is formulated as an EVRPTWPR model with multi-energy consumption rate scenarios. We refer to this problem as a multi-scenario EVRPTWPR. Since the route and load level decisions are non-adjustable variables, they should satisfy all scenarios in the given uncertainty set $\bar{\mathcal{U}}$. However, the arrival time, battery energy level, and battery charge level decisions can vary to deal with the different scenarios. We can easily infer that the multi-scenario EVRPTWPR is more challenging to solve than the single-scenario one. To deal with this computational challenge, we adopt one of the solution methods for solving the single-scenario EVRPTWPR, which is a hybrid variable neighbourhood search and tabu search (VNS-TS) metaheuristic with an annealing mechanism similar to the one used in Schneider et al. (2014). Such a solution method has the advantage of combining diversification and intensification features, which are key ingredients in the design of metaheuristics (Gendreau and Potvin, 2010). The diversification operators are the VNS shaking step (which can generate solutions structurally distant from the incumbent one) and the annealing mechanism (which can accept to move the search to an unimproved neighbour solution). The intensification operator relies on the tabu search metaheuristic that is applied to try to improve the solution provided by the VNS shaking step. The diversification features are able to explore new regions of the solution space, whereas the intensification operator is able to deeply investigate promising regions of the solution space. The combination of intensification/diversification features has been employed successfully in various VRP problems (e.g., Coindreau et al. (2019)).

In the following sections, we describe the VNS approach in detail, where all constants and variables in the corresponding violation functions are represented in the time unit. Thus, with abuse of notation, $h^s_{ij} \leftarrow g \times h^s_{ij} \times d_{ij}$ represents the time needed to recharge the consumed energy on an arc $(i, j)$ for scenario $\boldsymbol{h}^s$, and $B \leftarrow g \times B$ denotes the time needed to recharge the vehicle fully.

#### 4.2.1. Preprocessing, generalized cost function, and initial solution

For computational efficiency, we exclude infeasible arcs as done by Schneider et al. (2014) and Schiffer and Walther (2018). The infeasibility of arc $(u, v)$ is determined by the following preprocessing constraints:

$$u, v \in P \wedge q_u + q_v > C \tag{8a}$$

$$u \in V_0, v \in V_{N+1} \wedge e_u + s_u + t_{uv} > l_v \tag{8b}$$

$$u \in V_0, v \in V \wedge e_u + s_u + t_{uv} + s_v + t_{v,N+1} > l_0 \tag{8c}$$

$$u, v \in P \wedge \forall i \in F_0, j \in F_{N+1} : h_{iu} + h_{uv} + h_{vj} > B \tag{8d}$$

$$u, v \in V_{0,N+1} \wedge h_{uv} > B. \tag{8e}$$

Constraints (8a)–(8c) identify infeasibility based on load capacity and time window violations. Constraints (8d) and (8e) identify infeasibility due to the battery capacity as discussed in Schneider et al. (2014) and Schiffer and Walther (2018), respectively. All infeasible arcs satisfying any of constraints (8) are removed from the arc set $A$. Additionally, at every CCG iteration, we remove infeasible arcs satisfying (8d) and (8e) when a new scenario is added to the set $\bar{\mathcal{U}}$.

As is commonly done, we allow infeasible solutions during the search. The approach of Schneider et al. (2014) considers the sum of the total travelled distance, total load capacity violation, time window violations, battery capacity violation, and the diversification penalty. Schiffer and Walther (2018) consider the total recharging time, time window violation, and battery capacity violation. Cortés-Murcia et al. (2019) evaluate the cost function as the sum of the time spent at recharging stations, time window violation, and battery capacity violations. In our approach, we define the generalized cost for a route $\mathcal{R}$ as follows:

$$GC(\mathcal{R}) = \max_{s \in I(\bar{\mathcal{U}})} \left\{ \sum_{k \in K} \sum_{i \in F} p^s_{ik} + \alpha \Big( TW^s(\mathcal{R}) + FL^s(\mathcal{R}) \Big) \right\} + \beta FR(\mathcal{R}), \tag{9}$$

where $p^s_{ik}$, $TW^s(\mathcal{R})$, and $FL^s(\mathcal{R})$ represent the energy recharged at station $i$ of vehicle $k$, time window violation of route $\mathcal{R}$, and battery capacity violation of route $\mathcal{R}$ for the $s$th scenario in set $\bar{\mathcal{U}}$, respectively. Function $FR(\mathcal{R})$ is the load capacity violation of route $\mathcal{R}$. All violation terms $TW, FL$, and $FR$ are scaled by the weighting factors $\alpha$ and $\beta$. These factors are initialized by $(\alpha_0, \beta_0)$, are dynamically updated during the search, and limited between a given lower bounds $(\alpha_{\min}, \beta_{\min})$ and upper bounds $(\alpha_{\max}, \beta_{\max})$. We note that route $\mathcal{R}$ is said to be *feasible* for a scenario $s$ if $TW^s(\mathcal{R}) = 0$, $FL^s(\mathcal{R}) = 0$, and $FR(\mathcal{R}) = 0$ and *robust feasible* for $\bar{\mathcal{U}}$ if route $\mathcal{R}$ is feasible for all scenarios $s \in I(\bar{\mathcal{U}})$.

To calculate the violations of the time window and battery capacity, we use the corridor-based penalty approach introduced in Schiffer and Walther (2018) and Cortés-Murcia et al. (2019). The time window and battery capacity violation are calculated as follows:

$$TW^s(\mathcal{R}) = \sum_{\rho \in \mathcal{R}} \left\{ \sum_{v \in \rho} \max\left\{ \min\left\{ a^{\min}_{s,v}, a^{\max}_{s,v} \right\} - l_v, 0 \right\} \right\} \qquad \forall s \in I(\bar{\mathcal{U}}) \tag{10a}$$

$$FL^s(\mathcal{R}) = \sum_{\rho \in \mathcal{R}} \left\{ \sum_{v \in \rho} \max\left\{ a^{\min}_{s,v} - a^{\max}_{s,v}, 0 \right\} \right\} \qquad \forall s \in I(\bar{\mathcal{U}}), \tag{10b}$$

where $\rho$ denotes the route of a given vehicle, $a^{\min}_{s,v}$ is the earliest allowed service start time at a vertex $v$ for scenario $\boldsymbol{h}^s \in \bar{\mathcal{U}}$, and $a^{\max}_{s,v}$ is the earliest service start time at a vertex $v$ if as much energy as possible is recharged at recharging stations visited before reaching $v$ for scenario $\boldsymbol{h}^s \in \bar{\mathcal{U}}$. Readers can refer to Schiffer and Walther (2018) and Cortés-Murcia et al. (2019) for additional details.

The load capacity violation of a route $\rho$ is calculated as follows:

$$FR(\mathcal{R}) = \sum_{\rho \in \mathcal{R}} \max\left\{ \sum_{v \in \rho} q_v - C, 0 \right\}. \tag{11}$$

We note that the load capacity violation is calculated in $\mathcal{O}(1)$ for any case where the route $\mathcal{R}$ is updated (Schneider et al., 2014; Schiffer and Walther, 2018; Cortés-Murcia et al., 2019).

We construct an initial solution using the approach in Lin et al. (2021). We first choose an arbitrary point and calculate all angles between the depot, this random point, and all the customers. All customers are sorted in ascending order of the angle value. Then, a customer is iteratively inserted into an active route at the position causing the smallest energy consumption increment. The route becomes inactive when any customer insertion causes a violation in the time window or battery capacity, and another route is activated to insert the remaining customers. The number of available employed vehicles is given as a parameter. If there still remain any unrouted customers and no more routes can be activated, the remaining customers are inserted into the last route disregarding any time window and batter capacity violation.

#### 4.2.2. Variable neighbourhood search and tabu search components

The variable neighbourhood search (VNS) was proposed by Mladenović and Hansen (1997) for the travelling salesman problem, and several other research followed and proposed some variations (e.g., Bierlaire et al., 2010; Schneider et al., 2014; Cortés-Murcia et al., 2019; Thevenin and Zufferey, 2019; Lin et al., 2021). From the provided literature, it was shown that the VNS can find near-optimal solutions, and sometimes optimal solutions, for the EVRPTWPR, and more generally for highly complex optimization problems. Next, we extend the VNS-TS approach proposed by Schneider et al. (2014) to solve the master problem, [RMP($\bar{\mathcal{U}}$)], which is a multi-scenario EVRPTWPR. The VNS approach proceeds as follows: given a current solution $\mathcal{R}$, a neighbouring solution $\mathcal{R}'$ is generated by a cyclic-exchange operator. It selects a random number $n_r$ of routes from $\mathcal{R}$. An arbitrary length of consecutive vertices is chosen to form an exchange block. These blocks are reversed and transferred between selected routes. The neighbouring solution $\mathcal{R}'$ defined by the exchange of blocks could be feasible or not.

In line with other work on VNS (e.g., Thevenin et al., 2017), a tabu search (TS) is used for a local search strategy to improve the neighbouring solution $\mathcal{R}'$. For each VNS iteration, TS is run for $n_{tabu}$ iterations, and it provides a new set of routes $\mathcal{R}''$. If the $\mathcal{R}''$ is an improving solution compared to $\mathcal{R}$, then $\mathcal{R}$ is replaced by $\mathcal{R}''$. However, even if the $\mathcal{R}''$ is not an improving solution, it can be accepted depending on the acceptance criteria based on simulated annealing (SA) (Kirkpatrick et al., 1983). Specifically, the non-improving solution $\mathcal{R}''$ is accepted with a probability of $e^{(GC(\mathcal{R})-GC(\mathcal{R}''))/T}$, where $T$ is temperature of annealing phase. Temperature $T$ is initialized by $T_0$ to accept non-improving solution $\mathcal{R}''$ with the probability of 50% when $GC(\mathcal{R}'')$ is $\Delta_{SA}$ worse than $GC(\mathcal{R})$. For every VNS iteration, the temperature linearly decreases. We apply the same parameter settings used by Lin et al. (2021).

In line with the VRP neighbourhood search structures proposed in the literature (see for example Golden et al., 2008), six operators are applied to the solution $\mathcal{R}'$, such as 2-opt*, exchange-intra, exchange-inter, relocate-intra, relocate-inter, and stationInRe. Each operator has its own tabu set. The best none-tabu move is chosen. The move is said to be superior if the resulting solution has a lower cost function value or is a robust feasible solution with fewer employed vehicles. The operators that are applied are described as follows.

- 2-opt*: Select two routes $\rho_i$ and $\rho_j$, and split them into two partial routes, i.e., $\rho_i \rightarrow \rho_i^1, \rho_i^2$ and $\rho_j \rightarrow \rho_j^1, \rho_j^2$. Then, construct two new routes such as $\rho_i^{new} \leftarrow \rho_i^1 + \rho_j^2$ and $\rho_j^{new} \leftarrow \rho_j^1 + \rho_i^2$.
- Exchange-intra: Select two vertices $i$ and $j$ from a route $\rho = \langle 0, \dots, i^-, i, \dots, j^-, j, \dots, N+1 \rangle$. Then, exchange the positions of them, such that $\rho^{new} = \langle 0, \dots, i^-, j, \dots, j^-, i, \dots, N+1 \rangle$.
- Exchange-inter: Select a vertex $i$ from route $\rho_i$ and a vertex $j$ from route $\rho_j$. Exchange the positions of them, such that $\rho_i^{new} = \langle 0, \dots, i^-, j, i^+ \dots, N+1 \rangle$ and $\rho_j^{new} = \langle 0, \dots, j^-, i, j^+ \dots, N+1 \rangle$.
- Relocate-intra: Select vertices $i$ and $j$ from route $\rho$. Delete $i$ from $\rho$ and reinsert it after $j$, such that $\rho^{new} = \langle 0, \dots, i^-, i^+, \dots, j, i, j^+, \dots, N+1 \rangle$.
- Relocate-inter: Select a vertex $i$ from route $\rho_i$ and a vertex $j$ from route $\rho_j$. Delete $i$ from $\rho_i$ and reinsert it after $j$ of $\rho_j$, such that $\rho_i^{new} = \langle 0, \dots, i^-, i^+, \dots, N+1 \rangle$ and $\rho_j^{new} = \langle 0, \dots, j, i, j^+, \dots, N+1 \rangle$.
- stationInRe: Select an unassigned station vertex and insert it into the route or remove a station vertex in the route.

Note that, $i^-$ and $i^+$ represent the preceding and succeeding vertices of the vertex $i$. Each operator considers all possible vertices and positions. Then, the best move is chosen, and the removed edges by this best move are stored in the corresponding operator's tabu set. Each operator cannot consider the reinsertion of an edge if the edge is in its tabu set. Every edge in the tabu set has its tabu tenure which is randomly chosen from a range of $\left[n_{tabu}^{\min}, n_{tabu}^{\max}\right]$, where $n_{tabu}^{\min}$ and $n_{tabu}^{\max}$ are parameters that will be tuned in the computational results.

### 4.3. Solution method for the subproblem

Recall subproblem [SP($\boldsymbol{x}^*$)] presented in Section 4.1. We add slack variables $\boldsymbol{w} = (\boldsymbol{w}_1, \boldsymbol{w}_2)$ and their objective term $\boldsymbol{\kappa}^\top \boldsymbol{w}$ as given in the problem below:

$$\max_{\boldsymbol{h}\in\mathcal{U}} \min_{\boldsymbol{y}} \quad \boldsymbol{b}^\top \boldsymbol{y} + \boldsymbol{\kappa}^\top \boldsymbol{w} \tag{12a}$$

$$\text{s.t. } \boldsymbol{F}\boldsymbol{y} \le \boldsymbol{f} + \boldsymbol{w}_1 \tag{12b}$$

$$\boldsymbol{H}\boldsymbol{y} \le \boldsymbol{g} - \boldsymbol{G}(\boldsymbol{h})\boldsymbol{x}^* + \boldsymbol{w}_2, \tag{12c}$$

where $\boldsymbol{w} = (\boldsymbol{w}_1, \boldsymbol{w}_2)$ and $\boldsymbol{\kappa} = (\boldsymbol{\kappa}_1, \boldsymbol{\kappa}_2)$ are the vector of slack variables and their objective coefficients, respectively. As mentioned in Section 4.1, slack variables are added to guarantee the feasibility of [SP($\boldsymbol{x}^*$)]. Since the subproblem (12) has a bilevel structure, it cannot be solved directly. We note that the inner minimization problem is a linear programming problem, and it can be dualized as a maximization problem. Then, the resulting problem can be represented as follows:

$$\max_{\boldsymbol{h},\lambda,\boldsymbol{\varphi}} \quad \boldsymbol{\varphi}^\top \big(\boldsymbol{G}(\boldsymbol{h})\boldsymbol{x}^* - \boldsymbol{g}\big) - \lambda^\top \boldsymbol{f} \tag{13a}$$

$$\text{s.t. } \quad -\lambda^\top \boldsymbol{F} - \boldsymbol{\varphi}^\top \boldsymbol{H} \le \boldsymbol{b}^\top \tag{13b}$$

$$\boldsymbol{0} \le \lambda \le \boldsymbol{\kappa}_1 \tag{13c}$$

$$\boldsymbol{0} \le \boldsymbol{\varphi} \le \boldsymbol{\kappa}_2 \tag{13d}$$

$$\boldsymbol{h} \in \mathcal{U}, \tag{13e}$$

where $\lambda$ and $\boldsymbol{\varphi}$ are the dual multipliers of the constraints (7b) and (7c), respectively, and vectors $\boldsymbol{\kappa}_1$ and $\boldsymbol{\kappa}_2$ are the subvectors of $\boldsymbol{\kappa}$ for $\boldsymbol{w}_1$ and $\boldsymbol{w}_2$, respectively. Note that the dualized subproblem (13) is a bilinear optimization problem with a bilinear term $\boldsymbol{\varphi}^\top \boldsymbol{G}(\boldsymbol{h})\boldsymbol{x}^*$ in the objective function. Since the bilinear terms only exist in the objective function and its feasible region can be separated for $(\lambda, \boldsymbol{\varphi})$ and $\boldsymbol{h}$, thus problem (13) is a separable bilinear program. The optimal solution of problem (13) consists of the extreme point of the polyhedron $\{(\lambda, \boldsymbol{\varphi}) : -\lambda^\top \boldsymbol{f} - \boldsymbol{\varphi}^\top \boldsymbol{H} \le \boldsymbol{b}^\top, \boldsymbol{0} \le \lambda \le \boldsymbol{\kappa}_1, \boldsymbol{0} \le \boldsymbol{\varphi} \le \boldsymbol{\kappa}_2\}$ and the extreme point of the uncertainty set $\mathcal{U}$. Therefore, we can solve subproblem (13) using the alternating direction (AD) algorithm proposed by Konno (1976). The AD algorithm always converges to a Karush–Kuhn–Tucker (KKT) point of problem (13) (Lorca and Sun, 2014). The AD algorithm iteratively solves two problems; one is (13) with a fixed $\boldsymbol{h}$ and the other is the same problem (13) with a fixed $(\lambda, \boldsymbol{\varphi})$. Details are summarized in Algorithm 2.

**Algorithm 2** Alternating Direction (AD) Algorithm

1: $\tilde{\boldsymbol{h}} \leftarrow \bar{\boldsymbol{h}}$
2: $LB \leftarrow 0$, $UB \leftarrow \infty$
3: **while** $UB - LB < \varepsilon$ **do**
4: $\quad LB \leftarrow \max_{(\lambda,\boldsymbol{\varphi})\in\Pi} \boldsymbol{\varphi}^\top \big(\boldsymbol{G}(\tilde{\boldsymbol{h}})\boldsymbol{x}^* - \boldsymbol{g}\big) - \lambda^\top \boldsymbol{f}$ and let $(\lambda^*, \boldsymbol{\varphi}^*)$ be its optimal solution ▷ $\Pi := \{(\lambda, \boldsymbol{\varphi}) : (13b)\text{–}(13e)\}$
5: $\quad UB \leftarrow \max_{\boldsymbol{h}\in\mathcal{U}} \boldsymbol{\varphi}^{*\top} \big(\boldsymbol{G}(\boldsymbol{h})\boldsymbol{x}^* - \boldsymbol{g}\big) - \lambda^{*\top} \boldsymbol{f}$ and let $\boldsymbol{h}^*$ be its optimal solution
6: $\quad \tilde{\boldsymbol{h}} \leftarrow \boldsymbol{h}^*$
7: $\zeta^* \leftarrow UB$

### 4.4. Proposed solution framework

In the previous sections, we introduced the different components of our approach: the CCG method, the VNS-TS algorithm, and the AD algorithm. The general CCG method iteratively solves the relaxed master problem to optimality and detects a scenario defining the worst violation. In other words, multi-scenario EVRPTWPR has to be solved several times, and the size of the problem increases as the CCG iteration number increases. Therefore, we can easily infer that our multi-scenario EVRPTWPR suffers computational difficulties compared to the single-scenario EVRPTWPR. To avoid computational intractability, we propose to solve the relaxed master problem until a robust feasible solution is obtained from the VNS-TS approach and then solve the subproblem to obtain a violated scenario. Thus we do not wait for the VNS-TS to terminate to solve the subproblem as that is time consuming.

Thus, the proposed solution method starts from an uncertainty set with only a nominal energy consumption rate scenario $\bar{\mathcal{U}} = \{\bar{\boldsymbol{h}}\}$. The VNS-TS algorithm is used to find a robust feasible route for $\bar{\mathcal{U}}$. If any robust feasible route is found, then the subproblem is solved to detect a scenario defining the worst violation. The detected scenario is added to the uncertainty set $\bar{\mathcal{U}}$. Once a scenario is added, the current robust feasible route can be infeasible or have a higher cost. As a result, the VNS-TS continues from the previous solution to find a new robust feasible route for the updated uncertainty set or to improve the current route. The stopping criteria of the VNS-TS algorithm is that route $\mathcal{R}$ should be robust feasible for the uncertainty set $\bar{\mathcal{U}}$ and that the gap between the value of the generalized cost function $GC(\mathcal{R})$ and the objective value of the subproblem is less than a predefined threshold. We summarize the proposed algorithm in Algorithm 3.

**Algorithm 3** Proposed Algorithm Based on CCG framework

1: $\bar{\mathcal{U}} \leftarrow \{\tilde{\boldsymbol{h}}\}$
2: $i \leftarrow 0$
3: $UB \leftarrow \infty$
4: $x \leftarrow \text{InitialSolution}(\bar{\mathcal{U}})$
5: **while True do**
6: $\quad x' \leftarrow \text{cyclic-exchange}(x)$
7: $\quad x'' \leftarrow \text{TabuSearch}(x')$
8: $\quad$ **if** $GC(x'') \leq UB$ **then**
9: $\quad\quad i \leftarrow 0$
10: $\quad\quad x \leftarrow x''$
11: $\quad\quad$ **if** $x''$ is robust feasible for $\bar{\mathcal{U}}$ **then**
12: $\quad\quad\quad \zeta^*, \tilde{\boldsymbol{h}} \leftarrow \text{AlternatingDirection}(x'')$
13: $\quad\quad\quad$ **if** $\zeta^* - GC(x'') < \delta$ **then**
14: $\quad\quad\quad\quad x''$ is the best robust feasible solution for $\mathcal{U} \rightarrow$ Terminate Algorithm
15: $\quad\quad\quad$ **else**
16: $\quad\quad\quad\quad UB \leftarrow GC(x'')$
17: $\quad\quad\quad\quad \bar{\mathcal{U}} \leftarrow \bar{\mathcal{U}} \cup \{\tilde{\boldsymbol{h}}\}$
18: $\quad$ **else if** $\text{acceptSA}(x, x'')$ **then**
19: $\quad\quad x \leftarrow x''$
20: $\quad$ **if** $x''$ is robust feasible for $\bar{\mathcal{U}}$ **then**
21: $\quad\quad \zeta^*, \tilde{\boldsymbol{h}} \leftarrow \text{AlternatingDirection}(x'')$
22: $\quad\quad$ **if** $\zeta^* - GC(x'') < \delta$ **then**
23: $\quad\quad\quad x''$ is the best robust feasible solution for $\mathcal{U} \rightarrow$ Terminate Algorithm
24: $\quad$ **else**
25: $\quad\quad i \leftarrow i + 1$
26: $\quad\quad$ **if** $i > n_{feas}$ **then**
27: $\quad\quad\quad$ No robust feasible solution $\rightarrow$ Terminate Algorithm

Instead of using the VNS-TS algorithm to find the best solution for the multi-scenario EVRPTWPR which might require several iterations, we use the VNS-TS approach to obtain a robust feasible route for the uncertainty set $\bar{\mathcal{U}}$ and generate a new violated scenario to obtain an updated [RMP($\bar{\mathcal{U}}$)]. This decreases the computational requirements of the proposed method.

We note that Algorithm 3 guarantees to find a robust feasible solution for AR-EVRPTWPR (2). This can be achieved in two cases: when a robust optimal solution is found or when a robust feasible solution is found. The former is evident. A robust optimal solution $\boldsymbol{x}^*$ of [RMP($\bar{\mathcal{U}}$)] provides a lower bound on AR-EVRPTWPR since an uncertainty set $\bar{\mathcal{U}}$ is a subset of the uncertainty set $\mathcal{U}$. We note that the subproblem [SP($\boldsymbol{x}^*$)] provides an upper bound. Thus, a robust optimal solution $\boldsymbol{x}^*$ of [RMP($\bar{\mathcal{U}}$)] is a robust optimal solution of AR-EVRPTWPR when the stopping criterion at Step 14 or 23 in Algorithm 3 is satisfied. In the latter case, even if Algorithm 3 fails to find a robust optimal solution for [RMP($\bar{\mathcal{U}}$)], an obtained solution $\boldsymbol{x}''$ is still a robust feasible solution for [RMP($\bar{\mathcal{U}}$)]. This solution is not a lower bound on AR-EVRPTWPR, but since we have slack variables $\boldsymbol{w}$ in [SP($\boldsymbol{x}''$)], and their objective coefficients are relatively huge (e.g., $\kappa$ is set as 10000 for each entry), any violation caused by infeasibility gives a large objective value of [SP($\boldsymbol{x}''$)]. Thus, a satisfaction of the stopping criterion at Step 14 or 23 denotes that a robust feasible solution $\boldsymbol{x}'$ of [RMP($\bar{\mathcal{U}}$)] is also a robust feasible solution for AR-EVRPTWPR. In other words, Algorithm 3 can be terminated with a robust feasible solution of AR-EVRPTWPR even when [RMP($\bar{\mathcal{U}}$)] and [SP($\boldsymbol{x}''$)] are not solved optimally. We note that since we are using a heuristic we cannot guarantee the optimality of the resulting solution, however from Section 5 we can show that the proposed approach has high-quality robust solutions for this problem.

## 5. Computational experiments

This section presents extensive computational results to illustrate the performance of the proposed AR-EVRPTWPR solution approach. We first show the results related to the proposed Algorithm 3 for the AR-EVRPTWPR. Then, Monte-Carlo simulation tests are conducted to evaluate the economic impact and robustness of the routes obtained from the ARO model compared to that of the deterministic model.

The AR-EVRPTWPR is first applied to small-sized instances of Schneider et al. (2014) to demonstrate the quality of solutions obtained using our algorithm. We compare these results with the ones obtained from the commercial solver CPLEX. Next, we generate mid-sized instances to show the computational capability of our algorithm. These mid-sized instances are generated as follows. We randomly pick 20, 30, and 40 customers from the large-sized instances of Schneider et al. (2014). Then, we solve the created mid-sized instances using the VNS-TS metaheuristic five times, and the visited stations in the shortest route are chosen to be the recharging stations for these instances. We note that this instance generation is similar to how (Schneider et al., 2014) generated the small-sized instances.

**Table 3**
Comparing CCG using CPLEX with the proposed approach.

| *Inst.* | CCG with CPLEX | | | | | Proposed Algorithm 3 | | | | | | |
|---|---|---|---|---|---|---|---|---|---|---|---|---|
| | $n_v$ | *worst* | *dist.* | *t(s)* | *iter.* | $n_v$ | *worst* | *dist.* | *t(s)* | *iter.* | $gap_w$(%) | $gap_d$(%) |
| C101C5 | 2 | 277.47 | 257.75 | 219.89 | 3 | 2 | 277.47 | 257.75 | 0.48 | 7 | 0 | 0 |
| C103C5 | 1 | 190.02 | 176.12 | 4.10 | 5 | 1 | 190.02 | 176.12 | 0.39 | 9 | 0 | 0 |
| C206C5 | 1 | 269.36 | 250.28 | 2121.17 | 10 | 1 | 269.36 | 250.28 | 0.73 | 8 | 0 | 0 |
| C208C5 | 1 | 179.88 | 164.34 | 205.35 | 10 | 1 | 179.88 | 164.34 | 0.41 | 7 | 0 | 0 |
| R104C5 | 2 | 148.00 | 137.25 | 171.68 | 4 | 2 | 148.00 | 137.25 | 0.34 | 5 | 0 | 0 |
| R202C5 | 1 | 154.66 | 143.29 | 216.54 | 7 | 1 | 154.66 | 143.29 | 0.39 | 8 | 0 | 0 |
| R203C5 | 1 | 193.13 | 179.06 | 81.97 | 2 | 1 | 193.13 | 179.06 | 0.32 | 9 | 0 | 0 |
| RC105C5 | 2 | 260.58 | 241.30 | 118.29 | 6 | 2 | 260.58 | 241.30 | 3.79 | 107 | 0 | 0 |
| RC108C5 | 2 | 274.38 | 253.93 | 13.79 | 4 | 2 | 274.38 | 253.93 | 0.40 | 4 | 0 | 0 |
| RC204C5 | 1 | 191.99 | 176.40 | 70.67 | 11 | 1 | 191.99 | 176.40 | 0.38 | 5 | 0 | 0 |
| RC208C5 | 1 | 189.42 | 173.57 | 12.53 | 10 | 1 | 189.42 | 173.57 | 1.13 | 14 | 0 | 0 |
| C101C10 | 3 | 415.82 | 393.56 | 9024.16 | 5 | 3 | 415.82 | 393.56 | 46.63 | 67 | 0 | 0 |
| C104C10 | 2 | 304.25 | 287.84 | 10800* | 5 | 2 | 290.21 | 273.93 | 22.02 | 56 | −4.61 | −4.83 |
| C202C10 | 2 | 266.88 | 251.95 | 10800* | 5 | 2 | 267.21 | 252.05 | 24.88 | 50 | 0.12 | 0.04 |
| C205C10 | 2 | 245.18 | 231.97 | 10800* | 5 | 2 | 245.18 | 231.97 | 67.99 | 120 | 0 | 0 |
| R102C10 | 4 | 275.96 | 262.93 | 10800* | 5 | 4 | 275.96 | 262.93 | 2.67 | 7 | 0 | 0 |
| R201C10 | 2 | 240.19 | 228.41 | 7226.32 | 4 | 2 | 240.19 | 228.41 | 26.79 | 78 | 0 | 0 |
| RC108C10 | | | T | | | 3 | 378.71 | 357.23 | 13.74 | 58 | – | – |
| RC201C10 | 2 | 385.67 | 363.53 | 10800* | 7 | 2 | 377.27 | 355.89 | 15.99 | 91 | −2.18 | −2.10 |
| RC205C10 | | | T | | | 2 | 391.42 | 368.99 | 1.56 | 4 | – | – |
| C103C15 | | | T | | | 3 | 396.16 | 380.14 | 98.80 | 56 | – | – |
| C106C15 | | | T | | | 3 | 378.75 | 361.53 | 73.58 | 75 | – | – |
| C202C15 | | | T | | | 3 | 394.48 | 377.95 | 217.01 | 131 | – | – |
| C208C15 | 2 | 322.30 | 306.25 | 10800* | 5 | 2 | 318.04 | 300.55 | 28.02 | 54 | −1.32 | −1.86 |
| R102C15 | | | T | | | 5 | 456.66 | 441.13 | 648.25 | 372 | – | – |
| R105C15 | | | T | | | 4 | 368.63 | 353.93 | 74.28 | 57 | – | – |
| R202C15 | | | T | | | 3 | 401.33 | 386.28 | 138.33 | 113 | – | – |
| R209C15 | 2 | 420.43 | 403.51 | 10800* | 5 | 2 | 322.07 | 307.68 | 65.97 | 61 | −23.40 | −23.75 |
| RC103C15 | | | T | | | 4 | 416.26 | 397.75 | 114.84 | 72 | – | – |
| RC108C15 | | | T | | | 3 | 399.11 | 378.35 | 26.81 | 61 | – | – |
| RC202C15 | | | T | | | 3 | 418.01 | 397.20 | 382.40 | 237 | – | – |
| RC204C15 | 2 | 432.52 | 412.47 | 10800* | 5 | 2 | 327.65 | 310.81 | 69.22 | 38 | −24.25 | −24.65 |

The following sections show that considering uncertainty could provide significantly different results than the deterministic model with a small change in the energy consumption rate. For instance, the simulation results show that the routes from the deterministic model are infeasible in many cases, but the proposed ARO model shows higher feasibility even for small $\Gamma$ values.

### 5.1. Experimental setup

For the computational experiments, all considered models and algorithms are implemented in Python and performed on a server with an Intel Xeon Silver 4114 CPU. CPLEX 20.1.0 is used as the optimization solver.

For the parameter settings, all CPLEX parameters are kept to the default values. The convergence tolerance for the CCG framework is set as $\delta = 0.001$. The objective coefficient vector $\boldsymbol{\kappa}$ of the subproblem is set as 10000 for each entry. Since the objective value of the subproblem can be huge in the case of infeasibility, the stopping criterion for the AD algorithm is set as $(UB - LB)/LB < 0.0001$. For the VNS-TS algorithm, the number of VNS iterations is limited to $n_{feas} = 500$ for all sizes of instances. The penalty parameters $(\alpha, \beta)$ are set to $(\alpha_0, \beta_0) = (10, 10)$, $(\alpha_{min}, \beta_{min}) = (1, 1)$ and $(\alpha_{max}, \beta_{max}) = (5000, 5000)$. The penalty parameters $(\alpha, \beta)$ increase or decrease by 1.2 times every two continuous infeasible and feasible VNS iterations, respectively. For the simulated annealing based acceptance criteria, $\Delta_{SA}$ is set to 10. For the tabu search, the lower and upper bounds of tabu tenure are set as $n_{tabu}^{min} = 15$ and $n_{tabu}^{max} = 30$, respectively.

A set of homogeneous EVs is considered, where each EV has a battery capacity $B$ equal to 77.75 and a load capacity $C$ of 200. In this case, a set of homogeneous recharge stations is considered, where the recharging rate $g_i$ is 1.0 for all $i \in F$. In addition, the expected energy consumption rate $\bar{h}_a$ is set to 1.0 for all arcs. We note that all these values are the same as the small-sized instances of Schneider et al. (2014). In addition, we allow each vehicle to re-visit the same recharging station at most once (i.e., $\nu = 1$).

### 5.2. Computational results

The computational performance of the proposed Algorithm 3 is reported in Table 3. We compare CCG using CPLEX with Algorithm 3 in terms of solution time and quality for small-sized instances of Schneider et al. (2014). For CCG with CPLEX, the RMP is solved to optimality using CPLEX for each CCG iteration, and the AD algorithm solves the subproblem as presented in Algorithm 2. The computational time is limited to 10,800 CPU seconds for both the CCG with CPLEX and for Algorithm 3 and $\Gamma$ is set to

**Table 4**
Results for mid-sized instances.

| *Inst.* | Deterministic model | | ARO model | | | |
|---|---|---|---|---|---|---|
| | $n_v$ | *dist.* | $n_v$ | *worst* | *dist.* | $t(s)$ |
| C101C20 | 4 | 466.63 | 4 | 483.50 | 466.82 | 284.34 |
| C103C20 | 4 | 381.83 | 4 | 399.85 | 383.25 | 292.53 |
| C206C20 | 2 | 412.79 | 2 | 445.18 | 425.61 | 233.35 |
| C208C20 | 2 | 376.61 | 2 | 491.58 | 472.31 | 205.88 |
| R104C20 | 4 | 337.26 | 5 | 378.64 | 364.36 | 187.87 |
| R105C20 | 6 | 505.07 | 7 | 568.12 | 549.28 | 230.75 |
| R203C20 | 2 | 260.26 | 2 | 273.78 | 262.94 | 164.60 |
| RC105C20 | 8 | 654.70 | 8 | 685.80 | 664.26 | 232.39 |
| RC108C20 | 6 | 520.83 | 6 | 569.25 | 546.25 | 1065.22 |
| RC204C20 | 2 | 410.26 | 4 | 428.56 | 409.91 | 174.72 |
| C101C30 | 5 | 739.64 | 5 | 772.66 | 750.45 | 5739.58 |
| C104C30 | 4 | 459.00 | 4 | 476.02 | 460.69 | 750.46 |
| C202C30 | 3 | 516.28 | 3 | 548.84 | 530.79 | 761.65 |
| C205C30 | 3 | 539.84 | 3 | 560.57 | 540.56 | 463.27 |
| R102C30 | 7 | 604.75 | 8 | 603.36 | 585.64 | 1214.53 |
| R103C30 | 8 | 740.98 | 9 | 790.43 | 774.16 | 4715.54 |
| R201C30 | 3 | 567.26 | 3 | 626.90 | 609.70 | 4953.61 |
| R203C30 | 3 | 404.22 | 3 | 434.10 | 417.03 | 1099.81 |
| RC102C30 | 10 | 904.62 | 11 | 1031.00 | 999.94 | 5916.7 |
| RC205C30 | 4 | 629.98 | 4 | 663.83 | 644.97 | 947.61 |
| C103C40 | 5 | 685.23 | 5 | 729.52 | 712.29 | 2868.03 |
| C202C40 | 4 | 516.01 | 4 | 548.24 | 534.29 | 3935.44 |
| C208C40 | 4 | 524.94 | 4 | 539.22 | 525.31 | 4084.10 |
| R102C40 | 11 | 917.60 | 12 | 968.35 | 947.42 | 2479.40 |
| R105C40 | 10 | 821.08 | 11 | 905.94 | 887.3 | 932.01 |
| R202C40 | 4 | 570.40 | 4 | 600.98 | 585.45 | 1179.85 |
| R209C40 | 4 | 499.92 | 4 | 515.84 | 503.04 | 3194.52 |
| RC108C40 | 10 | 874.35 | 11 | 955.82 | 933.09 | 3858.94 |
| RC202C40 | 4 | 834.36 | 5 | 761.95 | 741.65 | 2759.23 |
| RC204C40 | 4 | 598.25 | 4 | 622.11 | 605.76 | 1534.38 |

6. We note that there are four small-sized instances where the robust feasible solution does not exist for the given uncertainty set ($\hat{h}_a = 0.1\bar{h}_a$, $\forall a \in \mathcal{A}$ and $\Gamma = 6$). There is one in the 5-customer instance (i.e., R105C5) and three in the 10-customer instance (i.e., R103C10, R203C10, and RC102C10).

In Table 3, column "*Inst.*" represents the instance's name, and the last value in each instance's name represent the number of customers (i.e., 5, 10, and 15). Column "$n_v$" denotes the number of employed vehicles. Columns "*worst*" and "*dist.*" records the worst-case energy consumption and the total distance of routes, respectively. Column "$t(s)$" reports the total CPU time in seconds. Column "*iter.*" represents the number of CCG iterations at the end of the used methods. Finally, columns "$gap_w$" and "$gap_d$" represent the increment of Algorithm 3 compared to the results of the CCG with CPLEX in terms of worst-case energy consumption and the total distance of routes, respectively. Let $w_1$ and $w_2$ be the worst energy consumption of solution from CCG with CPLEX and CCG with the proposed Algorithm 3, respectively. The $gap_w$ is calculated as $(w_2 - w_1)/w_1$. Similarly, let $d_1$ and $d_2$ be the travel distance of the solution from CCG with CPLEX and with the proposed Algorithm 3, respectively. Then, $gap_d = (d_2 - d_1)/d_1$. Both of them are reported in percentage. The "10800*" in the $t(s)$ column denotes that the algorithm fails to terminate within the time limit. For these cases, we report the results of the best robust feasible solution found. Finally, "T" indicates that the algorithm fails to find any robust feasible solution within the time limit.

Results in Table 3 show the proposed Algorithm 3 is promising to solve the AR-EVRPTWPR. The CCG framework using CPLEX can solve all of the instances with 5-customers. On the other hand, it can find robust feasible solutions for 7 out of the 9 instances with 10 customers and fails to find any robust feasible solution for most instances with 15 customers. However, Algorithm 3 can find robust feasible solutions for all small-sized instances within a reasonable computational time. Except for only one instance (i.e., C202C10), the proposed Algorithm 3 finds robust optimal or near-optimal solutions. Also, it can provide better solutions compared to the robust feasible solutions that the CCG with CPLEX finds within the time limit. For instance, the best robust feasible solution found by the proposed Algorithm 3 has 24.65% shorter travel distance (at RC204C15) than the solution provided by the CCG with CPLEX, and the computational time was only 69.22 s.

Table 4 reports the computational results for mid-sized instances. Column "Deterministic model" represents the number of employed vehicles and travel distances when energy consumption rate uncertainty is not considered. Column "ARO model" denotes the results of AR-EVRPTWPR consisting of the number of employed vehicles, worst-case energy consumption, travel distance, and computational time. For the uncertainty set, the $\Gamma$ is set to 6 and $\hat{h}_a = 0.1\bar{h}_a$, $\forall a \in \mathcal{A}$. The computational time limit is set to 10,800 CPU seconds.

Table 4 illustrates that the proposed Algorithm 3 can solve all mid-sized instances within the time limit. The computational time increases as the instance's size increases, and most of the computational time is less than two hours. Results in Table 4 also show

**Table 5**
Simulation results — Normal distribution considering correlation.

| *Inst.* | $n_v$ | $\Gamma$ | Avg. | Std. | Max | Min | Feasibility(%) |
|---|---|---|---|---|---|---|---|
| C103C40 | 5 | 0 | 739.31 | 76.06 | 1181.19 | 654.88 | 37.8 |
| | 5 | 6 | 735.72 | 41.18 | 923.20 | 679.99 | 54.0 |
| | 5 | 12 | 715.40 | 15.11 | 887.35 | 682.68 | 97.2 |
| C202C40 | 4 | 0 | 526.05 | 29.45 | 716.56 | 493.75 | 79.6 |
| | 4 | 6 | 534.63 | 8.03 | 590.34 | 510.83 | 99.4 |
| | 4 | 12 | 553.94 | 7.60 | 577.61 | 528.94 | 100 |
| C208C40 | 4 | 0 | 524.56 | 6.93 | 548.57 | 505.15 | 100 |
| | 4 | 6 | 524.96 | 7.11 | 548.14 | 503.18 | 100 |
| | 4 | 12 | 530.86 | 7.07 | 555.14 | 510.39 | 100 |
| R102C40 | 11 | 0 | 1050.95 | 184.36 | 2124.14 | 854.53 | 24.2 |
| | 12 | 0 | 1043.61 | 156.06 | 1901.64 | 867.58 | 27.2 |
| | 12 | 6 | 986.83 | 80.95 | 1430.77 | 878.82 | 53.6 |
| | 12 | 12 | 968.18 | 60.97 | 1341.97 | 879.75 | 59.1 |
| R105C40 | 10 | 0 | 901.28 | 110.71 | 1600.49 | 767.45 | 29.0 |
| | 11 | 0 | 911.00 | 116.12 | 1701.84 | 772.83 | 28.7 |
| | 11 | 6 | 907.21 | 55.27 | 1327.24 | 827.66 | 68.9 |
| | 11 | 12 | 911.10 | 45.08 | 1173.85 | 841.42 | 70.9 |
| R202C40 | 4 | 0 | 606.05 | 55.75 | 903.26 | 547.75 | 49.0 |
| | 4 | 6 | 587.89 | 13.56 | 703.34 | 562.71 | 93.7 |
| | 4 | 12 | 589.04 | 14.36 | 724.95 | 559.99 | 94.6 |
| R209C40 | 4 | 0 | 500.48 | 8.91 | 593.97 | 476.77 | 98.2 |
| | 4 | 6 | 503.43 | 8.17 | 585.27 | 480.85 | 98.8 |
| | 4 | 12 | 524.19 | 7.97 | 619.76 | 499.61 | 99.4 |
| RC108C40 | 10 | 0 | 979.76 | 131.23 | 1559.45 | 816.64 | 26.0 |
| | 11 | 0 | 1025.77 | 158.27 | 1769.91 | 827.88 | 19.8 |
| | 11 | 6 | 958.80 | 65.32 | 1316.57 | 860.96 | 63.4 |
| | 11 | 12 | 1006.53 | 60.99 | 1356.31 | 911.71 | 67.7 |
| RC202C40 | 4 | 0 | 922.03 | 104.96 | 1407.59 | 796.82 | 25.2 |
| | 5 | 0 | 747.21 | 57.38 | 1073.74 | 687.80 | 71.0 |
| | 5 | 6 | 742.94 | 15.60 | 908.80 | 706.06 | 95.2 |
| | 5 | 12 | 761.68 | 10.00 | 789.06 | 726.57 | 100 |
| RC204C40 | 4 | 0 | 602.43 | 18.87 | 752.61 | 574.57 | 90.1 |
| | 4 | 6 | 605.92 | 8.31 | 653.53 | 577.83 | 99.5 |
| | 4 | 12 | 615.79 | 7.88 | 660.27 | 593.01 | 99.5 |

that the routes become more conservative than the deterministic ones. In most cases, the travel distances increase. Also, in some instances, the required number of vehicles is higher than the deterministic model. The increased travel distances and employed EVs can be interpreted as follows: to withstand the energy consumption rate uncertainties, the employed vehicles should visit more recharging stations or fewer customers than in the deterministic case.

From the results of Tables 3 and 4, we can demonstrate that the proposed Algorithm 3 is able to find a robust feasible solution that is close to the robust optimal solution. Furthermore, the computational time is reasonable for instances with 40 customers.

### 5.3. Economical impact and robustness

This section studies the economic efficiency and robustness of the ARO model by conducting Monte-Carlo simulation tests for 40-customer instances. We generated a set of 1000 energy consumption rate scenarios using three probability distributions: normal distribution (ND), uniform distribution (UD), and normal distribution considering correlation (NDC). For ND and UD, the energy consumption rate of arc $a$, $h_a$, is sampled from the normal distribution with $\mu = \bar{h}_a, \sigma = 0.1\bar{h}_a$ and the uniform distribution with the range $[0.9\bar{h}_a, 1.1\bar{h}_a]$, respectively. For NDC, Lee et al. (2012) assume that customers in congested areas tend to have more travel time than customers in other areas. Similarly, we postulate that arcs located close to one another have similar energy consumption rate uncertainty. Thus, $h_a$ is defined as $\bar{h}_a + \bar{h}_a(z_i + z_j)$, where $z_a$ follows $\mathcal{N}\left(0, \left(\frac{0.1}{2\sqrt{2}}\right)^2\right)$ for all arcs $a \in \mathcal{A}$.

Since deterministic or robust routes can be infeasible for some scenarios, we use the generalized cost function $GC(\mathcal{R})$ in (9) to evaluate the route's costs. In the simulation tests, $\alpha$ and $\beta$ in the generalized cost function $GC(\mathcal{R})$ are set to $(1, 10)$. For example, if route $\mathcal{R}$ is feasible for scenario $s_1$, its cost will be the electric energy needed to complete EVs' travel (i.e., $GC(\mathcal{R}) = \sum_{k\in K, i\in F} p_{ik}$). However, if route $\mathcal{R}$ is infeasible for scenario $s_2$, its cost will be the sum of required energy and penalties (i.e., $GC(\mathcal{R}) = \sum_{k\in K, i\in F} p_{ik} + 10 \times (TW^{s_2}(\mathcal{R}) + FL^{s_2}(\mathcal{R}) + FR(\mathcal{R}))$).

Tables 5, 6, and 7 report the simulation results for NDC, ND, and UD, respectively. Column "$\Gamma$" represents the considered value of budget uncertainty value in Eq. (3). A model with $\Gamma = 0$ denotes the deterministic model. Columns "Avg." and "Std." represent the average route's costs and the standard deviation of the route's costs. Columns "Max" and "Min" represent the largest and smallest route's cost among 1000 scenarios. To show how the budget of uncertainty affects the robustness, we report the results of two ARO

**Table 6**
Simulation results — Normal distribution.

| *Inst.* | $n_v$ | $\Gamma$ | Avg. | Std. | Max | Min | Feasibility(%) |
|---|---|---|---|---|---|---|---|
| C103C40 | 5 | 0 | 807.6 | 138.81 | 1583.96 | 648.69 | 23.4 |
| | 5 | 6 | 762.5 | 76.78 | 1155.82 | 671.94 | 47.5 |
| | 5 | 12 | 723.73 | 36.21 | 1018.05 | 678.69 | 85.8 |
| C202C40 | 4 | 0 | 543.15 | 58.65 | 870.45 | 491.49 | 67.6 |
| | 4 | 6 | 538.24 | 20.94 | 710.38 | 505.69 | 91.4 |
| | 4 | 12 | 554.42 | 13.36 | 697.6 | 526.54 | 98.1 |
| C208C40 | 4 | 0 | 524.72 | 8.79 | 558.58 | 494.28 | 99.7 |
| | 4 | 6 | 525.38 | 8.85 | 552.52 | 492.43 | 99.9 |
| | 4 | 12 | 531.57 | 8.90 | 558.28 | 498.27 | 100 |
| R102C40 | 11 | 0 | 1181.63 | 207.84 | 2177.63 | 883.31 | 5.3 |
| | 12 | 0 | 1138.62 | 178.29 | 2034.79 | 886.22 | 9.8 |
| | 12 | 6 | 1036.07 | 112.16 | 1665.16 | 906.9 | 31.3 |
| | 12 | 12 | 1013.62 | 96.04 | 1473.5 | 904.82 | 34.3 |
| R105C40 | 10 | 0 | 989.18 | 148.65 | 1705.83 | 779.64 | 10.2 |
| | 11 | 0 | 995.98 | 152.66 | 1719.47 | 777.5 | 11.4 |
| | 11 | 6 | 952.12 | 92.38 | 1466.38 | 845.67 | 39.7 |
| | 11 | 12 | 953.44 | 84.52 | 1456.37 | 851.42 | 40.2 |
| R202C40 | 4 | 0 | 632.53 | 87.68 | 1068.21 | 543.23 | 43.1 |
| | 4 | 6 | 606.42 | 52.02 | 942.59 | 556.72 | 70.8 |
| | 4 | 12 | 597.37 | 34.08 | 835.21 | 550.43 | 81.6 |
| R209C40 | 4 | 0 | 508.47 | 33.24 | 766.05 | 475.85 | 88.5 |
| | 4 | 6 | 509.58 | 29.94 | 744.6 | 474.47 | 92.4 |
| | 4 | 12 | 527.35 | 19.69 | 766.51 | 494.48 | 94 |
| RC108C40 | 10 | 0 | 1067.62 | 172.8 | 2013.18 | 838.98 | 12.6 |
| | 11 | 0 | 1129.68 | 187.01 | 2153.56 | 854.94 | 6.5 |
| | 11 | 6 | 1018.84 | 117.12 | 1588.53 | 881.13 | 32.7 |
| | 11 | 12 | 1077.39 | 122.02 | 1783.43 | 937.13 | 35.4 |
| RC202C40 | 4 | 0 | 1027.29 | 182.75 | 2045.43 | 786.35 | 12.3 |
| | 5 | 0 | 792.86 | 115.78 | 1383.88 | 674.52 | 53.7 |
| | 5 | 6 | 758.73 | 53.58 | 1215.99 | 694.5 | 79.3 |
| | 5 | 12 | 766.68 | 24.19 | 963.26 | 719.13 | 91.8 |
| RC204C40 | 4 | 0 | 617.84 | 49.19 | 936.13 | 564.66 | 71.8 |
| | 4 | 6 | 607.79 | 16.35 | 784.17 | 575.47 | 95.8 |
| | 4 | 12 | 616.74 | 16.25 | 838.54 | 581.63 | 97.1 |

models with $\Gamma = 6$ and $\Gamma = 12$ and compare them with the deterministic model. In addition, there are some cases where the ARO model employs more EVs. For those instances and to have a fair comparison, we also report the results of a deterministic model that uses the same number of EVs.

The results in Tables 5, 6, and 7 show the following. First, a route from the ARO model has a higher chance of being completed without battery capacity issues. For all probability distributions, the ARO models' results indicate higher feasibility than the deterministic model. For instance, in the case of C103C40 and uniform distribution, the deterministic model is only feasible at 35.4%. Still, the ARO model with $\Gamma = 12$ is feasible for most scenarios except two. Also, even if the ARO model's feasibility is low, it is at least 2.2 times higher than the deterministic model (as seen for R102C40 instance in Table 5) and reaches 6.5 times (for the same R102C40 instance in Table 6). Second, the results of the deterministic model show higher volatility than ARO models. We can see that the ARO models show a lower std for all cases, and its magnitude ranges from 1.1 (R209C40 in Table 5) to 13.2 times (RC202C40 in Table 7). The high value of the std can be interpreted as the insecurity of the route. In other words, there could be more risk of failure to complete servicing customers or risk of paying more charging costs than expected. The ARO models with $\Gamma = 12$ usually have lower std values than the ARO models with $\Gamma = 6$. Lastly, more employed EVs cannot guarantee robustness. For instances R102C40, R105C40, RC108C40, and RC202C40, ARO models employ one additional EV to find their robust solution. Except for the instance of RC202C40, the other three instances show that the deterministic model provides similar results whether an additional EV is employed or not. In RC202C40, even if additional EVs can provide a more robust route, the results are still worse than the ARO model. For instance, a route employing 5 EVs of the deterministic model shows 71% feasibility and 57.38 MWh for std, but a route of the ARO model with $\Gamma = 12$ shows 100% feasibility and 10 MWh for std (see Table 5).

To provide additional managerial insights, we choose one mid-sized instance (C103C40) and illustrate the route of each model in terms of the amount of electricity charging en route, travel ending times, and idle times. We first visualize the routes of the five EVs for three cases in Fig. 1, where $S_i$ represents a recharging station, and $S_0$ is the depot. Fig. 1(a) represents the EVs' routes of the deterministic model ($\Gamma = 0$), and Figs. 1(b) and 1(c) represent the routes of ARO models with $\Gamma = 6$ and $\Gamma = 12$, respectively. We can observe that each EV visits slightly different customers and stations for each model. In all three models, the total number of visited stations is the same. However, the number of visited customers for each EV is different for each model. For instance, for the deterministic model, the five EVs visit 7, 9, 9, 7, and 8 customers in order of EV1 to EV5. On the other hand, for the ARO

**Table 7**
Simulation results — Uniform distribution.

| *Inst.* | $n_v$ | $\Gamma$ | Avg. | Std. | Max | Min | Feasibility(%) |
|---|---|---|---|---|---|---|---|
| C103C40 | 5 | 0 | 739.03 | 67.78 | 1036.19 | 665.46 | 35.4 |
| | 5 | 6 | 735.61 | 39.17 | 916.03 | 689.3 | 56.4 |
| | 5 | 12 | 714.83 | 7.08 | 768.01 | 692.08 | 99.8 |
| C202C40 | 4 | 0 | 523.72 | 22.90 | 676.86 | 501.50 | 80.9 |
| | 4 | 6 | 534.14 | 5.28 | 551.46 | 516.01 | 99.8 |
| | 4 | 12 | 553.49 | 5.32 | 572.52 | 537.16 | 100 |
| C208C40 | 4 | 0 | 524.81 | 5.06 | 539.40 | 511.50 | 100 |
| | 4 | 6 | 525.50 | 4.94 | 541.52 | 509.99 | 100 |
| | 4 | 12 | 531.12 | 5.06 | 547.28 | 516.28 | 100 |
| R102C40 | 11 | 0 | 1019.24 | 90.88 | 1390.84 | 893.74 | 12.2 |
| | 12 | 0 | 1018.97 | 84.91 | 1451.93 | 910.17 | 16.6 |
| | 12 | 6 | 981.84 | 52.09 | 1210.18 | 921.16 | 47.5 |
| | 12 | 12 | 959.03 | 34.7 | 1141.24 | 916.99 | 60.7 |
| R105C40 | 10 | 0 | 884.93 | 69.17 | 1213.68 | 799.75 | 21.8 |
| | 11 | 0 | 895.02 | 73.81 | 1231.86 | 804.69 | 22.7 |
| | 11 | 6 | 900.52 | 32.26 | 1083.69 | 866.46 | 72.2 |
| | 11 | 12 | 904.2 | 24.07 | 1047.31 | 873.99 | 77.4 |
| R202C40 | 4 | 0 | 598.56 | 43.49 | 799.6 | 552.54 | 51.9 |
| | 4 | 6 | 586.39 | 8.18 | 692.99 | 568.61 | 97.3 |
| | 4 | 12 | 587.54 | 7.65 | 660.87 | 569.93 | 97.7 |
| R209C40 | 4 | 0 | 500.09 | 6.42 | 587.13 | 484.23 | 99.5 |
| | 4 | 6 | 503.14 | 6.34 | 592.08 | 489.24 | 99.5 |
| | 4 | 12 | 523.94 | 5.18 | 542.28 | 505.40 | 99.9 |
| RC108C40 | 10 | 0 | 963.13 | 88.27 | 1337.97 | 847.89 | 18.7 |
| | 11 | 0 | 1009.42 | 97.87 | 1524.18 | 864.14 | 12 |
| | 11 | 6 | 946.31 | 31.76 | 1163.8 | 907.45 | 70.9 |
| | 11 | 12 | 998.57 | 32.13 | 1153.84 | 954.78 | 70.3 |
| RC202C40 | 4 | 0 | 912.81 | 93.49 | 1320.14 | 805.52 | 25.3 |
| | 5 | 0 | 746.75 | 51.55 | 1034.57 | 700.84 | 70 |
| | 5 | 6 | 742.9 | 11.6 | 836.07 | 716.96 | 95.1 |
| | 5 | 12 | 761.85 | 7.09 | 782.61 | 737.85 | 100 |
| RC204C40 | 4 | 0 | 600.61 | 12.34 | 714.16 | 580.96 | 92.3 |
| | 4 | 6 | 605.94 | 5.87 | 625.34 | 589.74 | 99.9 |
| | 4 | 12 | 615.61 | 5.67 | 631.65 | 598.37 | 100 |

models with $\Gamma = 6$ the number of customers for each EV is: 6, 8, 9, 7, and 10 customers and for $\Gamma = 12$ there are: 8, 8, 9, 7, and 8 customers.

Figs. 2, 3, and 4 illustrate the box plots of the total recharging amount en routes, the average travel ending time, and the average idle time, respectively. We use the data from the simulation results presented in Tables 5, 6, and 7. For each model, only the feasible scenarios are used for the box plot. Fig. 2 shows that the total recharging amount en route increases as $\Gamma$ increases. Since we report only feasible scenarios, Fig. 2 can also be interpreted as the total recharging time. It means that routes from ARO models have more time flexibility for recharging than the deterministic ones. Thus, ARO models show higher feasibility than the deterministic model (see Tables 5, 6, 7). Fig. 3 shows that the average end-travel time of EVs decreases as $\Gamma$ increases. It denotes that routes of ARO models spend less time on the road than the deterministic model. Fig. 4 shows the average idle time of EVs. Average idle time also tends to decrease as $\Gamma$ increases. Additionally, we note that there might be scenarios in which EVs visit charging stations and do not use them which might result in unnecessary energy consumption. For uniform distribution (UC) and normal distribution considering correlation (NDC), this does not happen. This means that EVs always visit and use charging stations when needed. However, for normal distribution, this case occurs. For $\Gamma = 6$, the EV visits a charging station but does not use it in one scenario among 475 scenarios. The amount of wasted energy is 11.87 MWh. For the ARO model with $\Gamma = 12$, the EV visits a charging station but does not use it in two scenarios among 858 scenarios. The average amount of wasted energy is 21.87 MWh. The frequency of this happening is relatively low but it is worth investigating in future research. With the results of Figs. 3, and 4, we can demonstrate that the ARO model can provide a route that utilizes EV fleets more efficiently. More precisely, a route from the ARO model can charge more electricity en route, may spend less time waiting for the next visit, and may complete the service earlier than the deterministic model.

## 6. Conclusion

This paper presents an adaptive robust model for the electric vehicle routing problem with time window and partial recharging when the energy consumption rate exhibits uncertainty. We postulate that recharging decision can be made after the uncertainty realization to complete an EV's travel without any time window violation or negative battery level. Since recharging decisions can

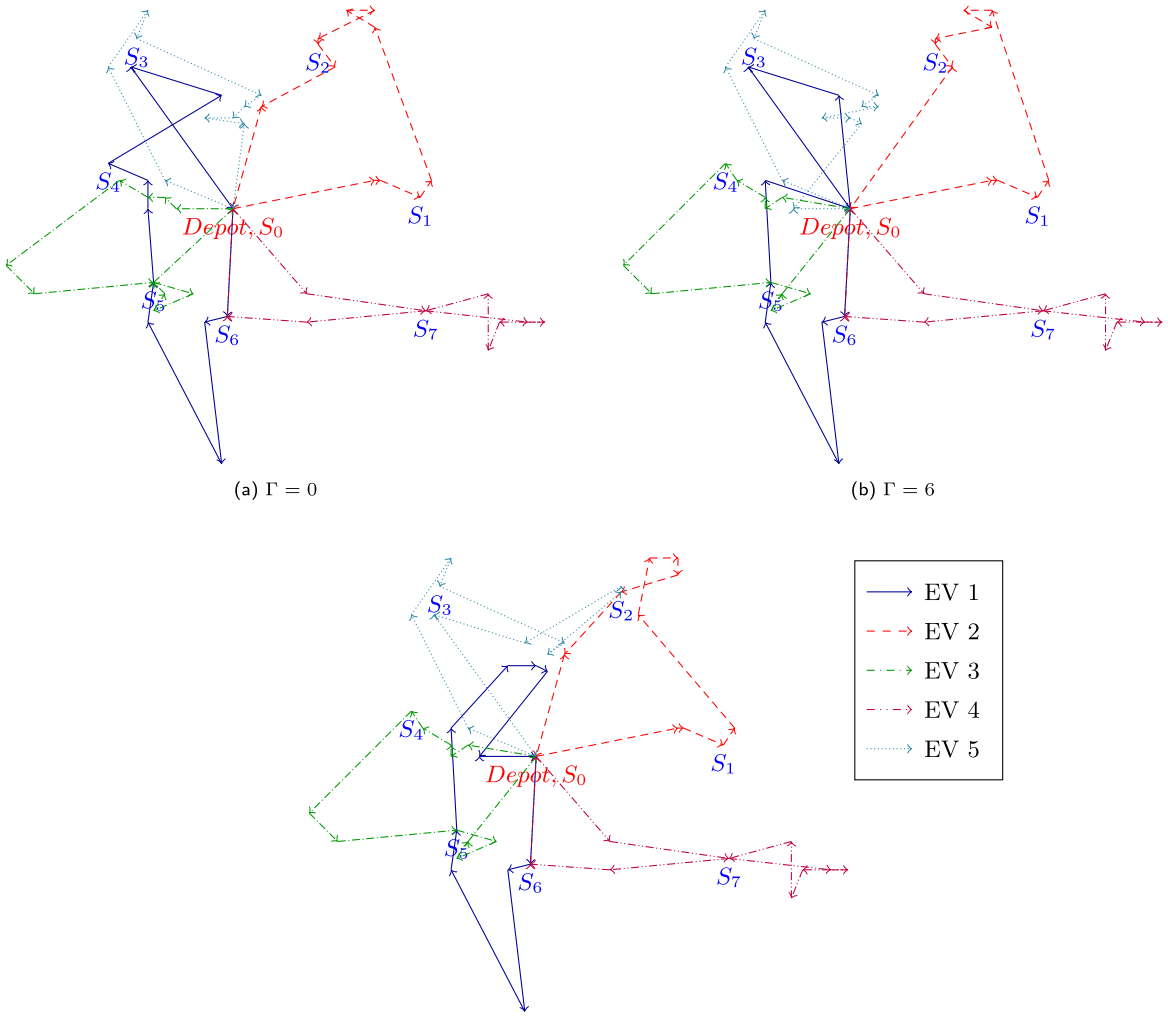


(a) $\Gamma = 0$ (b) $\Gamma = 6$

(c) $\Gamma = 12$

**Fig. 1.** EV routes — Instance of C103C40.

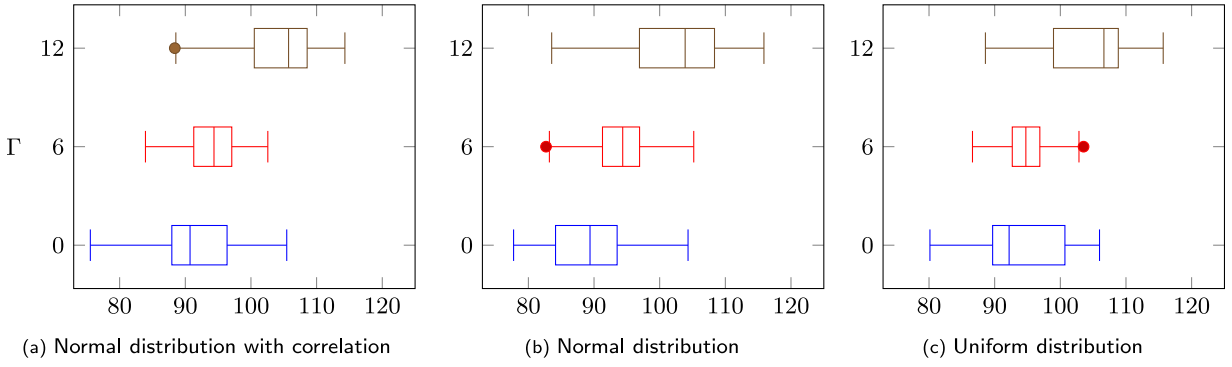


(a) Normal distribution with correlation (b) Normal distribution (c) Uniform distribution

**Fig. 2.** Total recharging amount (MWh).

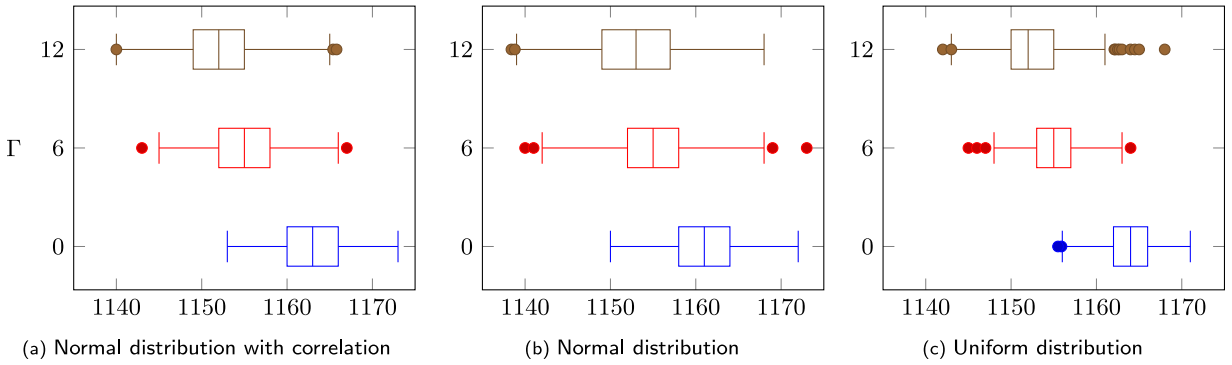


**Fig. 3.** Average travel ending time (min.).

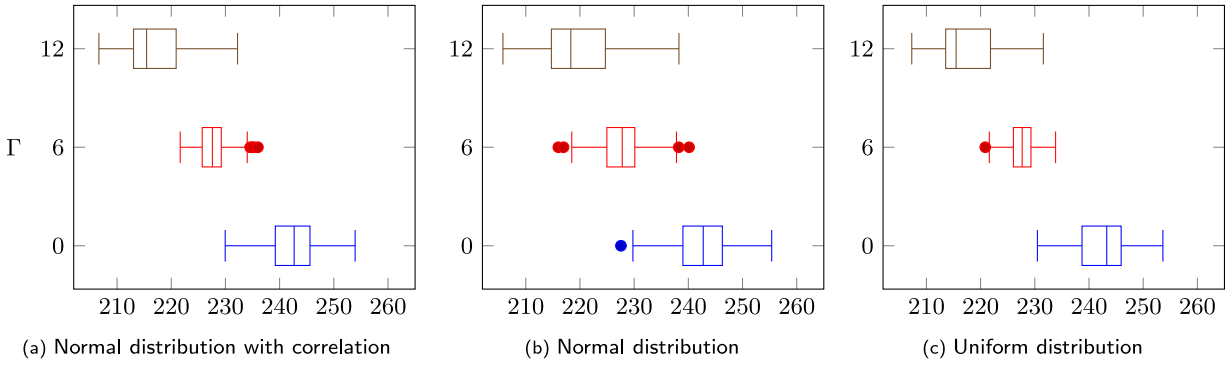


**Fig. 4.** Average idle time (min.).

affect other decisions, such as service start time and battery level at each vertex, the proposed model is formulated as a two-stage adaptive robust problem. A solution method based on the column-and-constraint generation framework has been proposed to solve our model in a reasonable computational time.

Small and mid-sized instances are used to demonstrate the advantage of the proposed model. Numerical results show the economic efficiency and robustness of the proposed model. Robust routes from our model may require more electrical energy compared to the deterministic model. However, they are more secure and reliable than the routes given by the deterministic model. In the adaptive robust model, there is a tradeoff between the expected amount of electricity charged and the robustness of routes. Decision makers can decide the proper tradeoff they need to consider to optimize their operations.

Additional features of the AR-EVRPTWPT model are worth investigating, such as using a nonlinear recharging function that leads to more realistic charging operations and accounting for the idle time at a given charging station in case of not charging. We will also look into developing an exact method for the proposed model to guarantee optimality. Additionally, extensive sensitivity analysis for the adaptive robust model with various uncertainty sets can be considered. As we mentioned in Section 5.3, uncertainties in the real world could be highly correlated. Furthermore, depending on the structure of the uncertainty set, there could be other relevant approaches to consider. Lastly, the time-variant uncertainty of energy consumption rate can be considered as future work. For example, when different EVs travel the same arcs but at different hours, each EV may have a different energy consumption rate. Therefore, introducing a time factor has practical significance since it could reflect more practical operations.

## CRediT authorship contribution statement

**Jaehee Jeong:** Data curation, Investigation, Software, Visualization, Writing – original draft. **Bissan Ghaddar:** Supervision, Conceptualization, Methodology, Writing – review & editing, Funding acquisition. **Nicolas Zufferey:** Supervision, Conceptualization, Writing – review & editing. **Jatin Nathwani:** Supervision, Conceptualization, Funding acquisition, Writing – review & editing.

## Acknowledgements

The authors thank the referees, the AE, and the Editor for their thorough and thoughtful comments. The authors also appreciate the funding support from Waterloo Institute for Sustainable Energy, Ontario, Canada. Bissan Ghaddar was supported by NSERC Discovery Grant 2017-04185.

## References


Agra, A., Christiansen, M., Hvattum, L.M., Rodrigues, F., 2018. Robust optimization for a maritime inventory routing problem. Transp. Sci. 52 (3), 509–525.

Basso, R., Kulcsár, B., Sanchez-Diaz, I., 2021. Electric vehicle routing problem with machine learning for energy prediction. Transp. Res. B 145, 24–55.

Basso, R., Kulcsár, B., Sanchez-Diaz, I., Qu, X., 2022. Dynamic stochastic electric vehicle routing with safe reinforcement learning. Transp. Res. Part E: Logist. Transp. Rev. 157, 102496.

Bektaş, T., Ehmke, J.F., Psaraftis, H.N., Puchinger, J., 2019. The role of operational research in green freight transportation. European J. Oper. Res. 274 (3), 807–823.

Ben-Tal, A., Golany, B., Nemirovski, A., Vial, J.-P., 2005. Retailer-supplier flexible commitments contracts: A robust optimization approach. Manuf. Serv. Oper. Manag. 7 (3), 248–271.

Ben-Tal, A., Goryashko, A., Guslitzer, E., Nemirovski, A., 2004. Adjustable robust solutions of uncertain linear programs. Math. Program. 99 (2), 351–376.

Bertsimas, D., Brown, D.B., Caramanis, C., 2011. Theory and applications of robust optimization. SIAM Rev. 53 (3), 464–501.

Bertsimas, D., Litvinov, E., Sun, X.A., Zhao, J., Zheng, T., 2012. Adaptive robust optimization for the security constrained unit commitment problem. IEEE Trans. Power Syst. 28 (1), 52–63.

Bierlaire, M., Thémans, M., Zufferey, N., 2010. A heuristic for nonlinear global optimization. INFORMS J. Comput. 22 (1), 59–70.

Bradley, T.H., Frank, A.A., 2009. Design, demonstrations and sustainability impact assessments for plug-in hybrid electric vehicles. Renew. Sustain. Energy Rev. 13 (1), 115–128.

Braekers, K., Ramaekers, K., Van Nieuwenhuyse, I., 2016. The vehicle routing problem: State of the art classification and review. Comput. Ind. Eng. 99, 300–313.

Coindreau, M.-A., Gallay, O., Zufferey, N., 2019. Vehicle routing with transportable resources: Using carpooling and walking for on-site services. Eur. J. Oper. Res. 279 (3), 996–1010.

Conrad, R.G., Figliozzi, M.A., 2011. The recharging vehicle routing problem. In: Proceedings of the 2011 Industrial Engineering Research Conference. IISE Norcross, GA, p. 8.

Cortés-Murcia, D.L., Prodhon, C., Afsar, H.M., 2019. The electric vehicle routing problem with time windows, partial recharges and satellite customers. Transp. Res. Part E: Logist. Transp. Rev. 130, 184–206.

Dantzig, G.B., Ramser, J.H., 1959. The truck dispatching problem. Manage. Sci. 6 (1), 80–91.

Dehghan, S., Amjady, N., Conejo, A.J., 2017. Adaptive robust transmission expansion planning using linear decision rules. IEEE Trans. Power Syst. 32 (5), 4024–4034.

Demir, E., Bektaş, T., Laporte, G., 2014. A review of recent research on green road freight transportation. European J. Oper. Res. 237 (3), 775–793.

Eksioglu, B., Vural, A.V., Reisman, A., 2009. The vehicle routing problem: A taxonomic review. Comput. Ind. Eng. 57 (4), 1472–1483.

Felipe, Á., Ortuño, M.T., Righini, G., Tirado, G., 2014. A heuristic approach for the green vehicle routing problem with multiple technologies and partial recharges. Transp. Res. Part E: Logist. Transp. Rev. 71, 111–128.

Froger, A., Jabali, O., Mendoza, J.E., Laporte, G., 2022. The electric vehicle routing problem with capacitated charging stations. Transp. Sci. 56 (2), 460–482.

Froger, A., Mendoza, J.E., Jabali, O., Laporte, G., 2019. Improved formulations and algorithmic components for the electric vehicle routing problem with nonlinear charging functions. Comput. Oper. Res. 104, 256–294.

Ge, M., Friedrich, J., Vigna, L., 2020. 4 charts explain greenhouse gas emissions by countries and sectors. World Resour. Inst. https://www.wri.org/insights/4-charts-explain-greenhouse-gas-emissions-countries-and-sectors. Accessed 29 August 2021.

Gendreau, M., Potvin, J.-Y., 2010. Handbook of Metaheuristics. Springer, Boston, MA.

GEOTAB, 2020. To What Degree Does Temperature Impact EV Range?. GEOTAB, Canada, https://www.geotab.com/blog/ev-range/. Accessed 27 August 2021.

Golden, B., Raghavan, S., Wasil, E., 2008. The Vehicle Routing Problem: Latest Advances and New Challenges. Springer, Boston, MA.

Gounaris, C.E., Wiesemann, W., Floudas, C.A., 2013. The robust capacitated vehicle routing problem under demand uncertainty. Oper. Res. 61 (3), 677–693.

Hiermann, G., Hartl, R.F., Puchinger, J., Vidal, T., 2019. Routing a mix of conventional, plug-in hybrid, and electric vehicles. European J. Oper. Res. 272 (1), 235–248.

IEA, 2021. Global EV Outlook 2021. IEA, Paris, https://www.iea.org/reports/global-ev-outlook-2021. Accessed 27 August 2021.

Keskin, M., Akhavan-Tabatabaei, R., Çatay, B., 2019. Electric vehicle routing problem with time windows and stochastic waiting times at recharging stations. In: 2019 Winter Simulation Conference. WSC, IEEE, pp. 1649–1659.

Keskin, M., Çatay, B., 2016. Partial recharge strategies for the electric vehicle routing problem with time windows. Transp. Res. C 65, 111–127.

Keskin, M., Çatay, B., Laporte, G., 2021. A simulation-based heuristic for the electric vehicle routing problem with time windows and stochastic waiting times at recharging stations. Comput. Oper. Res. 125, 105060.

Kirkpatrick, S., Gelatt, C.D., Vecchi, M.P., 1983. Optimization by simulated annealing. Science 220 (4598), 671–680.

Konno, H., 1976. A cutting plane algorithm for solving bilinear programs. Math. Program. 11 (1), 14–27.

Lee, C., 2021. An exact algorithm for the electric-vehicle routing problem with nonlinear charging time. J. Oper. Res. Soc. 72 (7), 1461–1485.

Lee, C., Lee, K., Park, S., 2012. Robust vehicle routing problem with deadlines and travel time/demand uncertainty. J. Oper. Res. Soc. 63 (9), 1294–1306.

Lin, C., Choy, K.L., Ho, G.T., Chung, S.H., Lam, H., 2014. Survey of green vehicle routing problem: past and future trends. Expert Syst. Appl. 41 (4), 1118–1138.

Lin, B., Ghaddar, B., Nathwani, J., 2021. Electric vehicle routing with charging/discharging under time-variant electricity prices. Transp. Res. C 130, 103285.

Lorca, A., Sun, X.A., 2014. Adaptive robust optimization with dynamic uncertainty sets for multi-period economic dispatch under significant wind. IEEE Trans. Power Syst. 30 (4), 1702–1713.

Mladenović, N., Hansen, P., 1997. Variable neighborhood search. Comput. Oper. Res. 24 (11), 1097–1100.

Montoya, A., Guéret, C., Mendoza, J.E., Villegas, J.G., 2017. The electric vehicle routing problem with nonlinear charging function. Transp. Res. B 103, 87–110.

Munari, P., Moreno, A., De La Vega, J., Alem, D., Gondzio, J., Morabito, R., 2019. The robust vehicle routing problem with time windows: compact formulation and branch-price-and-cut method. Transp. Sci. 53 (4), 1043–1066.

Pelletier, S., Jabali, O., Laporte, G., 2019. The electric vehicle routing problem with energy consumption uncertainty. Transp. Res. B 126, 225–255.

Pelletier, S., Jabali, O., Laporte, G., Veneroni, M., 2017. Battery degradation and behaviour for electric vehicles: Review and numerical analyses of several models. Transp. Res. B 103, 158–187.

Schiffer, M., Walther, G., 2017. The electric location routing problem with time windows and partial recharging. European J. Oper. Res. 260 (3), 995–1013.

Schiffer, M., Walther, G., 2018. An adaptive large neighborhood search for the location-routing problem with intra-route facilities. Transp. Sci. 52 (2), 331–352.

Schneider, M., Stenger, A., Goeke, D., 2014. The electric vehicle-routing problem with time windows and recharging stations. Transp. Sci. 48 (4), 500–520.

Sioshansi, R., Denholm, P., 2009. Emissions impacts and benefits of plug-in hybrid electric vehicles and vehicle-to-grid services. Environ. Sci. Technol. 43 (4), 1199–1204.

Statista, 2021. U.S. Vehicle Registrations 1990–2019. Statista, USA, https://www.statista.com/statistics/183505/number-of-vehicles-in-the-united-states-since-1990/. Published by Statista Research Department, 4 August 2021. Accessed 29 August 2021.

Sundström, O., Binding, C., 2010. Optimization methods to plan the charging of electric vehicle fleets. In: Proceedings of the International Conference on Control, Communication and Power Engineering. Citeseer, pp. 28–29.

Thevenin, S., Zufferey, N., 2019. Learning variable neighborhood search for a scheduling problem with time windows and rejections. Discrete Appl. Math. 261, 344–353.

Thevenin, S., Zufferey, N., Glardon, R., 2017. Model and metaheuristics for a scheduling problem integrating procurement, sale and distribution. Ann. Oper. Res. 259 (1), 437–460.

Toth, P., Vigo, D., 2014. Vehicle Routing: Problems, Methods, and Applications. SIAM.

US EPA, 2021. Fast Facts: U.S. Transportation Sector Greenhouse Gas Emissions, 1990–2019 (EPA-420-F-21-049, June 2021). EPA, U.S., https://nepis.epa.gov/Exe/ZyPDF.cgi?Dockey=P10127TU.pdf. United States Environmental Protection Agency, Accessed 29 August 2021.

Wang, Q., Watson, J.-P., Guan, Y., 2013. Two-stage robust optimization for $N-k$ contingency-constrained unit commitment. IEEE Trans. Power Syst. 28 (3), 2366–2375.

Winston, A., 2018. Inside UPS's electric vehicle strategy. Harv. Bus. Rev. URL https://hbr.org/2018/03/inside-upss-electric-vehicle-strategy.

Yanıkoğlu, İ., Gorissen, B.L., den Hertog, D., 2019. A survey of adjustable robust optimization. European J. Oper. Res. 277 (3), 799–813.

Yi, Z., Bauer, P.H., 2017. Effects of environmental factors on electric vehicle energy consumption: a sensitivity analysis. IET Electr. Syst. Transp. 7 (1), 3–13.

Yu, M., Nagarajan, V., Shen, S., 2022. Improving column generation for vehicle routing problems via random coloring and parallelization. INFORMS J. Comput. 34 (2), 953–973.

Yuksel, T., Michalek, J.J., 2015. Effects of regional temperature on electric vehicle efficiency, range, and emissions in the United States. Environ. Sci. Technol. 49 (6), 3974–3980.

Zang, Y., Wang, M., Qi, M., 2022. A column generation tailored to electric vehicle routing problem with nonlinear battery depreciation. Comput. Oper. Res. 137, 105527.

Zeng, B., Zhao, L., 2013. Solving two-stage robust optimization problems using a column-and-constraint generation method. Oper. Res. Lett. 41 (5), 457–461.

Zhang, J., Wang, Z., Liu, P., Zhang, Z., 2020. Energy consumption analysis and prediction of electric vehicles based on real-world driving data. Appl. Energy 275, 115408.